Scilight

Materials and Sustainability

https://www.sciltp.com/journals/matsus

Review

An Overview of the Transition from Amorphous Carbon to an Ordered Graphitic Crystalline Plane for Applications

Adriana Montiel-García [1], Manoj Kumar Srinivasan [2], Ignacio Avila Aguilar [1], Wilgince Apollon [1], Arun Thirumurugan [3] and Sathish-Kumar Kamaraj [1,*]

[1] Centro de Investigación en Ciencia Aplicada y Tecnología Avanzada (CICATA), Instituto Politécnico Nacional (IPN), Carretera Tampico-Puerto Industrial Altamira km 14.5, C. Manzano, Industrial Altamira, Altamira 89600, México
[2] Department of Biochemistry and Biotechnology, Faculty of Science, Annamalai University, Chidambaram 608002, India
[3] Sede Vallenar, Universidad de Atacama, Av. Costanera #105, Vallenar 1612178, Chile
* Correspondence: skamaraj@ipn.mx or sathish.bot@gmail.com

How To Cite: Montiel-García, A.; Srinivasan, M.K.; Aguilar, I.A.; et al. An Overview of the Transition from Amorphous Carbon to an Ordered Graphitic Crystalline Plane for Applications. *Materials and Sustainability* **2025**, *1*(3), 12. https://doi.org/10.53941/matsus.2025.100012

Received: 7 August 2025
Revised: 14 September 2025
Accepted: 17 September 2025
Published: 30 September 2025

Abstract: This review provides a comprehensive overview of the structural transformation from amorphous carbon—particularly in graphitizable soft carbons—to ordered graphitic crystalline planes, emphasizing the underlying mechanisms, advanced characterization techniques, and diverse applications. Carbon materials exhibit a broad spectrum of structures, from disordered amorphous forms to highly crystalline allotropes like graphite and graphene, with controlled transitions enabling tailored properties for energy storage, electronics, sensors, and composites. Key graphitization methods, including thermal annealing, catalytic processes, pressure-assisted techniques, and irradiation, are discussed in relation to processing conditions and resulting nanostructures. Thermodynamic and kinetic considerations, structural reorganization pathways, and the influence of heteroatoms and impurities are explored in depth. State-of-the-art characterization tools such as XRD, Raman spectroscopy, and TEM offer insights into atomic-scale studies. The review also addresses current challenges, emerging trends like sustainable and energy-efficient approaches, and future prospects for innovative carbon-based technologies.

Keywords: amorphous carbon; energy barriers; hybridization; thermal annealing

1. Introduction

Carbon materials are also endowed with an exceptional range of structures that go all the way from amorphous carbon (a-C) at one extreme to macroscopically grown crystalline allotropes like graphite, diamond, and graphene at the other [1]. This arrangement of the atomic structure gives rise to a wide range of different individual physical, chemical and electronic properties and these give carbon-based materials their pivotal role in most current applications of technology including electronics, catalysis, energy storage, and nanotechnology [2,3]. One of these structural transformations that have generated significant interest due to their possible practical uses, as well as to their ability to provide information on phase transitions and atomic ordering in carbon systems, is the conversion of amorphous carbon into graphitic forms [4].

Amorphous carbon lacks long-range order, featuring a mix of hybridization states, while graphitic carbon consists of ordered sp^2-hybridized layers. Thermal treatment is one of the most frequent ways to induce graphitisation. When heating amorphous carbon at high temperatures (above 2000 °C), it is possible to break down the regions of disorder, and the rearrangement of carbon atoms back into their sp^2 carbon hexagonal networks. The main phases which generally constitute the transformation are initial carbonisation (dehydration and elimination of the volatile species), structural reordering (generation of graphitic domains), and crystalline regions

development. Not all a-C materials are able to graphitise. Structural defects, heteroatoms, and amount of sp^3 bonding may hinder or distort graphitization pathway [5].

Graphitization is more feasible in soft carbons, derived from precursors with minimal cross-linking (e.g., petroleum pitch or cokes), which allow atomic rearrangement into graphitic structures. In contrast, hard carbons from cross-linked sources (e.g., resins or biomass) exhibit kinetic barriers that limit transformation to turbostratic or partially ordered forms, even at temperatures > 2500 °C [6,7].

Catalytic graphitization is another alternative method that will allow working at lower temperatures using metal catalysts such as iron, nickel or cobalt. These metals promote the break-down of the carbon atoms thereafter, to allow the re-precipitation of ordered graphs. It is often applied to the production of graphene and carbon nanotubes through amorphous carbon materials, and the shape and structure of the end product graphitised form can rely heavily on the catalyst [8].

Recent advances in characterisation methodologies have enabled more precise monitoring of the graphitization process at the atomic and nanoscopic scale to be performed in recent years. The techniques such as electron energy loss spectroscopy (EELS), transmission electron microscopy (TEM), Raman spectroscopy, and X-ray diffraction (XRD) cover bonding arrangements, crystallinity, zone size, and lattice orientation within the process of transformation. As an example, ratios between intensities of D and G bands in the Raman spectroscopy are particularly useful in distinction between disordered and orderly phases of carbon. On the same note, high-resolution TEM is able to identify turbostratic forms, or stacking faults and to see graphitic layer formation develop [9].

Also, computational modelling has been instrumental in elucidating the kinetics and thermodynamics of graphitization. The effect of defects and dopants in the process of ordering and the energy barriers due to rearrangement of bonds have been illuminated by calculations of density functional theory (DFT) and molecular dynamics simulations. These approaches in theory help to rationally construct protocols of transformations and complement experiments [10].

While previous reviews have provided valuable insights into the graphitization of amorphous carbon, such as comparative studies of transformation pathways [11] and greener alternatives for carbon nanomaterial synthesis [12], they often focus on specific aspects like molecular dynamics simulations or high-pressure effects without fully integrating emerging sustainability considerations. Recent works, including those on efficient conversion strategies for low-value precursors [13], highlight practical methods but lack comprehensive coverage of in-situ characterization and broad applications. This review distinguishes itself by offering a holistic synthesis that emphasizes sustainable, energy-efficient approaches (e.g., biomass-derived and low-energy catalytic processes), in-depth exploration of in-situ monitoring techniques for atomic-scale transformations, and a detailed comparison of graphitization methods, while addressing current challenges and future innovations in carbon-based technologies.

A huge potential of many possible applications lies in the ability to control the structural switching between amorphous and graphitic carbon. Graphitised carbon has high electrical conductivity and structural stability meaning that it finds application in energy storage, most often in lithium-ion battery cells and supercapacitors. Electronic applications of it are as interconnects, transistors, and conductive films. Also, to strengthen their mechanical properties and thermal conductivity, polymer composites are reinforced with graphitised carbon. Moreover, due to their high surface area and surface chemistry that is adjustable, graphitised nanostructures serve as chemical and bio sensor platforms [5,8].

2. Structural Diversity of Carbon Materials

Carbon is versatile due to the diversity of structures that it may create because of its flexibility in forming bonding configurations. All this is due to the ability of carbon to hybridise to sp, sp^2 or sp^3 states, adding to the large number of allotropes with different geometries and properties that it can form. This versatility gives rise to the rich structural diversity of carbon materials that can be roughly categorized into crystalline, amorphous and nanostructured.

2.1. Carbon Allotropes and Hybridization States

This is due to the ability of carbon to assume various hybridisation states which makes the formation of the various crystalline and nanostructured allotropes possible. The sp^3 hybridisation contributes to the structure of a diamond so that each carbon atom in the diamond has four tetrahedrally arranged sigma bonds in three-dimensional lattice. It is this highly ordered and rigid structural arrangement that makes diamond much harder to break, higher in melting point and in thermal conductivity [14]. Contrarily, the graphite consists of carbon atoms in the sp^2 state of hybridisation. In a 2-D hexagonal lattice, every atom has each carbon atom is covalently bonded with three other carbon, and has one valence electron. The weak van der Waals forces that align these graphene layers render

graphite anisotropic and soft, allowing the layers to glide over one another. The electrical conductivity occurs via covalent bonds and delocalised electrons, so that the layers can slide over each other [15]. Furthermore, carbon allotropes and the hybridisations that they represent are shown in a schematic way in Figure 1.

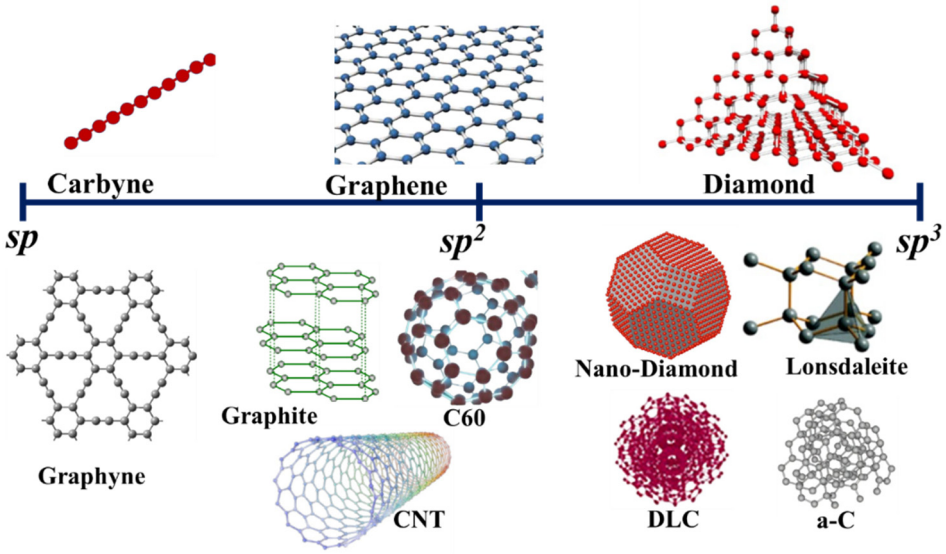

Figure 1. Allotropes of carbon and associated hybridisations and derivatives.

The bonding structure of the amorphous carbon is more intricate compared to these crystalline forms, where the carbon atoms get a mix of hybridisation states, i.e., sp^2, sp^3, and sometimes sp. These hybridisations have a considerable influence on the structure which results in properties of amorphous carbon [16]. Although more sp^2-containing have a higher electrical conductivity and are more graphite-like, materials with higher amounts of sp^3 are much more diamond like mechanically (as well as being referred to as diamond-like carbon, or al DLC [17]. Also, the numerous forms sp^2 carbon atoms can assume, as well as their curvature lead to diverse classes of nanostructured carbon material being obtained, such as fullerenes, carbon nanotubes, graphene, and turbostratic carbon [18]. Due to structural control by hybridisation Carbon materials are highly anisotropic and strongly display structural control due to hybridisation since these materials can be exceptionally different even when consisting of identical fundamental building blocks.

2.2. Amorphous Carbon Structures

Structurally disordered members of a class of carbon materials that lack long-range periodic order are called amorphous carbon. The atomic structure of amorphous carbon may differ widely, according to the synthesis methods, precursor substances, and conditions during treatment [19]. Included in this category is the tetrahedral amorphous carbon (ta-C) with composition between the sp^3-rich and more graphitic-like sp^2-dominated structures. Compared to that of crystalline carbon materials, the bond lengths and angles in amorphous carbon are spontaneous and this results in non-homogeneous network [20].

Localized structural features in amorphous carbon are aromatic clusters, aliphatic chains and cross linked carbon atoms. Even though they never reach out into a crystalline lattice, such arrangements of the units greatly influence the properties of the material. As an example, amorphous carbon, which has more sp^2 carbons, is better electrically conducting and absorbs light than in the higher-sp^3 content [21]. The absence of long-range order does not require complete chaos, and the short- and medium-range order can be embodied as the nano-sized graphitic domains with the more disordered matrices [22].

The selection of a precursor material has a potent impact on the type of produced amorphous carbon. The amorphous carbons with varied sp^2/sp^3 ratios can be made through the thermal decomposition of organic polymers such as polyacrylonitrile, carbohydrates of biomass and hydrocarbon gas such as acetylene and methane. Thermal treatment, as well as pyrolysis temperature and deposition methods such as chemical vapour deposition (CVD) or pulsed laser deposition (PLD), control further the structure and characteristics. Modern characterisation methods and calculational models have elucidated these complex systems that exhibit disorder-to-localisation order interactions in amorphous carbon systems [23].

2.3. Graphitic Crystalline Structures

At the highly ordered end of the structural continuum is found graphitic carbon. This crystal structure is composed of planar sheets of sp^2 hybridised carbon atoms in a regular hexagonal pattern [24]. In ideal graphite, these are packed in the arrangement of A-B-A-B etc with an interlayer distance of approximately 3.35 Å. The 16 coordinated 1s-electron interlayer system provides excellent electrical and thermal conductivity in-plane and the lubricating properties and ease of cleavage in some planes are explained by the lack of strong interlayer forces [25]. Most graphitic materials are in fact, not truly graphitic in this structure because of the imperfections such as stacking faults, rotational disorder, in-plane defects and finite crystallite sizes. These structural flaws can have a significant effect on all important physical properties such as mechanical strength, electrical conductivity and heat behaviour. As such, there arises the need to determine the degree of graphitisation, particularly when it comes to applications in high-performance carbon materials [26].

Structural ordering in graphitic materials is often characterized by metrics such as the in-plane size of the crystallites (La), stacking height (Lc) and interlayer distance of d(002). In most cases, these parameters are determined using the Raman spectroscopy and X-ray diffraction (XRD), etc. [27]. Moreover, it uses a g-factor also referred to as graphitisation index, to provide a keen assessment of the ordering level [19]. These structural characteristics are directly connected with function characteristics; e.g., electrical and thermal conductivity are improved with greater crystallites and reduced spacing of the interlayers. Such parameters are also needed to control the conversion of the amorphous or partially ordered forms of carbon to highly graphitised forms by heat treatment or by catalytic graphitisation [28].

3. Mechanisms of Transformation from Amorphous to Graphitic Carbon

The conversion of amorphous to graphitic carbon can be seen as a fundamental structural reorganisation in which disordered carbon networks are driven to very highly ordered crystalline structures. It takes place through a series of intermediate states with numerous reorganisation channels and takes place in a great influence of heteroatoms and impurities. It is governed by the thermodynamic favorability as well as kinetic restraints. To be able to manipulate the level of graphitisation in engineered carbon materials, in order to be able to selectively develop engineered carbon material towards mechanical, thermal, and electronic uses, it is necessary to understand these mechanisms.

3.1. Thermodynamic and Kinetic Considerations

The transition from amorphous to graphitic carbon is energetically advantageous for graphitizable (soft) carbons because graphite is the most thermodynamically stable form of carbon under normal circumstances. However, for non-graphitizable (hard) carbons, kinetic barriers arising from structural features like high sp^3 hybridization or cross-linking prevent this transformation despite the thermodynamic preference. Soft carbons, typically from precursors with low oxygen content and minimal cross-linking (e.g., petroleum coke or pitch), exhibit sufficient atomic mobility during heating to overcome energy barriers and form graphite. In contrast, hard carbons from oxygen-rich or cross-linked sources (e.g., phenolic resins or certain biomasses) develop rigid, disordered networks that resist reorganization, leading to turbostratic or glassy structures even at extreme temperatures. This distinction is critical for applications like battery anodes, where hard carbons provide higher lithium storage capacity due to their porosity but lack the conductivity of graphitized soft carbons [29,30]. These energy-intensive rearrangements transform irregular, non-planar carbon networks into graphite's long, hexagonal structures. Significant activation energy is needed for such structural transitions, and this energy is usually provided by high-temperature treatments, which frequently reach temperatures of over 1000 °C. However, the change is neither uniform nor instantaneous (Presser et al., 2011. [31]). Rather, it moves through a convoluted sequence of metastable intermediates that capture the original amorphous structure as well as local energetic constraints.

The rate and pathway of transformation are greatly influenced by kinetic factors, including the degree of initial disorder, the mobility of carbon atoms, and the presence of structural defects. Sp^2-bonded regions cluster as a result of localised thermal fluctuations and atomic rearrangements, gradually growing and aligning over time [32]. These domains eventually start to stack like graphite in soft (graphitizable) carbons, which undergo a mesophase (liquid crystalline) intermediate phase during carbonization, enabling molecular alignment and mobility for ordered stacking. However, full graphitic order might only be attained with the help of catalysis or extended heat exposure. In hard (non-graphitizable) carbons, this mesophase does not form due to cross-linked structures, preventing significant stacking; even with catalysts or prolonged annealing, only minimal graphitic order is achieved, often resulting in turbostratic domains [33].

3.2. Structural Reorganization Pathways

Pathways from amorphous to graphitic carbon vary by precursor hybridization and conditions, with sp^2-rich materials favoring cluster enlargement and sp^3-dominated ones requiring bond reconfiguration (cross-ref to Section 2.1). Critically, the nucleation and growth model excels for uniform precursors but overlooks local heterogeneity, as evidenced in high-temperature annealing where graphitic nuclei expand unevenly [11]. In contrast, aromatic cluster coalescence is more applicable to biomass-derived carbons, enabling lower-energy transitions but risking incomplete ordering without catalysts [13]. Table 1 presents a comparison of four structural reorganization pathways Nucleation and Growth, Aromatic Cluster Coalescence, Layer-by-Layer Ordering, and Defect Healing highlighting their key mechanisms, advantages, limitations, precursor suitability, and energy requirements.

In contrast, for sp^3-dominated materials like tetrahedral amorphous carbon (ta-C), the transformation requires energy-intensive bond reconfiguration. Li et al. demonstrated Ni-catalyzed annealing of ta-C films, inducing crystalline transformation to graphene at 600–900 °C via metal-induced layer exchange, with graphene quality improving at higher temperatures but limited by Ni agglomeration and carbon oversaturation [34]. This highlights heterogeneous pathways in DLC transitions, where thin ta-C layers (e.g., 2 nm) yield 3–4 graphene layers, differing from bulk nucleation models and emphasizing catalyst thickness effects on defect healing (activation energies ~70–90 kJ/mol reduced by metal mediation).

In contrast, aromatic cluster coalescence is more applicable to biomass-derived carbons, enabling lower-energy transitions but risking incomplete ordering without catalysts [13].

Layer-by-layer models provide insights into stacking faults via in-situ TEM but undervalue kinetic barriers in defect healing. Overall, hybrid mechanisms—combining these under catalytic or pressure-assisted conditions—offer optimal control, though sustainability challenges persist, such as high energy use in thermal paths versus greener catalytic alternatives [e.g., electrochemical methods for low-value resources]. This comparison highlights the need for tailored approaches: thermal for high-purity graphite, catalytic for scalable nanostructures.

To delve deeper into the sp^3 to sp^2 transformation, energy barriers play a pivotal role in dictating pathway feasibility. For sp^3-dominated amorphous carbon (e.g., tetrahedral a-C), the initial step involves breaking sp^3 bonds, with activation energies typically ranging from 0.5–2.0 eV per atom, as calculated via DFT for thermal-induced rehybridization [35]. These barriers arise from the need to overcome tetrahedral stability, often lowered under pressure (<10 GPa) where sp^3 sites convert more readily to sp^2 without full graphitization [36]. In contrast, sp^2-rich precursors exhibit lower barriers (~0.3–1.0 eV) for cluster fusion, facilitating spontaneous ordering at temperatures >1000 °C, though impurities can elevate them by introducing steric hindrance [37].

Defect evolution further modulates these pathways, starting with vacancies and interstitials in amorphous matrices that coalesce into larger voids or heal into graphitic rings. During annealing, point defects (e.g., Stone-Wales) migrate and annihilate, reducing disorder as monitored by Raman D-band intensity decreases [38]. In catalytic graphitization, metal-induced defects (e.g., via Fe or Ni dissolution) accelerate evolution, transforming amorphous regions into ordered domains through carbide intermediates, with in-situ XRD showing defect density drops from ~10^{12} cm^{-2} to <10^{10} cm^{-2} [39]. Swift heavy ion irradiation simulations reveal defect cascades leading to localized graphitization, where initial amorphization gives way to sp^2 clustering [40].

Computational simulations, such as DFT and MD, validate these mechanisms while challenging oversimplified experimental models. ReaxFF MD simulations of amorphous carbon annealing replicate experimental graphitization rates, predicting $sp^3 \rightarrow sp^2$ conversions with barriers of ~1.2 eV, aligning with TEM-observed domain growth but highlighting overlooked heterogeneous kinetics [41]. Hybrid DFT-MD models for carbon film deposition confirm sp^2/sp^3 ratios from XPS data, yet challenge uniform nucleation by showing defect-driven pathways dominate under non-equilibrium conditions [42]. Ab initio MD of coal carbonization simulates heteroatom effects, validating XRD patterns but revealing experimental underestimation of vacancy roles in early stages [10]. These tools thus bridge gaps, e.g., by quantifying barrier reductions (up to 50%) in doped systems, urging refined models integrating spatial variability.

Table 2 outlines the key energy barriers and defect evolution metrics involved in sp^3 to sp^2 transformations, emphasizing both computational and experimental insights.

Table 1. Comparison of of Structural Reorganization Pathways.

Pathway Model	Key Mechanism	Advantages	Limitations	Suitable Precursors	Energy Requirement	Reference
Nucleation and Growth	Graphitic nuclei form and consume disordered carbon	Uniform crystallinity; scalable for bulk materials	Ignores spatial heterogeneity; high temperatures needed	sp^2-rich amorphous carbons	High (>2000 °C)	[43,44]
Aromatic Cluster Coalescence	Fusion of sp^2 clusters into domains	Lower energy; promotes aromatic ring stability	Incomplete stacking without aids; sensitive to impurities	Biomass or polymer-derived	Moderate (1000–1500 °C with catalysts)	[44,45]
Layer-by-Layer Ordering	Sequential in-plane then interlayer order	Captures stacking evolution; aligns with TEM observations	Overlooks initial bond breaks in sp^3-heavy materials	Nanostructured carbons (e.g., CNTs)	Variable; often catalytic	[44]
Defect Healing	Thermal rearrangement corrects irregularities	Applicable to imperfect graphites; defect-specific	Slow kinetics; not predictive for large-scale	All types, post-initial ordering	Low to moderate (add-on to other paths)	[44]

Table 2. Key Energy Barriers and Defect Evolution Metrics in sp^3 to sp^2 Transformations.

Aspect	Metric/Example	Value/Range	Method/Source	Validation/Challenge
Energy Barrier (sp^3 Bond Breaking)	Thermal rehybridization in ta-C	0.5–2.0 eV/atom	DFT [35]	Aligns with annealing experiments; challenges low-T assumptions
Energy Barrier (Cluster Fusion)	sp^2-rich a-C annealing	0.3–1.0 eV	MD [37]	Validates Raman data; highlights impurity effects overlooked in models
Defect Density Reduction	Vacancy healing in catalytic process	10^{12} to 10^{10} cm^{-2}	In-situ XRD [39]	MD confirms; challenges homogeneous nucleation
Defect Type Evolution	Point defects to graphitic rings	Migration energy ~0.8 eV	ReaxFF MD [41]	Validates TEM; reveals heterogeneous kinetics
Pressure Effect on Barrier	<10 GPa on $sp^3 \rightarrow sp^2$	Reduced by 20–50%	Ab initio MD [36]	Aligns with HP experiments; urges defect-inclusive models

3.3. Role of Heteroatoms and Impurities

Heterogroups and metal impurities are the most important factor in the process of graphitization, usually facilitating or inhibiting processes depending on the chemical identity, the bonding structure, and the spatial distribution of the heterogroup in the carbon structure. The known graphitization catalysts are transition metals e.g., iron, nickel, cobalt, and manganese [46]. These components can reduce the activation energy necessary to disorganize atoms in the material by facilitating the mobility of atoms of carbon and serving as nucleation sites. Catalytic graphitization can occur in a number of ways such as deposition and decomposition of metal carbide, precipitation and dissolution of carbon, and the straight templating of carbon films to metallic surfaces. Such mechanisms are especially useful in industrial processes since they reduce the temperature required to achieve graphitisation and support the enhancement of the development of the long-range order [28]. Conversely, non-metallic heteroatoms, such as nitrogen, oxygen and sulphur, known to disrupt graphitisation are effective when substituted into the carbon network. These constituents lead to structural stress and asymmetry of the bonds that make graphene layers not to match and overlap on top of each other [47]. Oxygen-hydrogen bonds are strong covalent bonds in particular, which favor the cross-links structurally in the amorphous framework and prohibit the ease of the mobility of the carbon atom to facilitate restructuring [48]. But in certain situations heteroatoms may also positively affect the process of graphitisation. As an example, nitrogen can enhance the ordering within specific structural domains by stabilising edge sites and promoting the development of aromatic rings. These heteroatoms have a strong influence on the effect that can be strongly altered by the concentration and bonding scheme [49].

Non-metallic heteroatoms like boron can enhance ordering by stabilizing edges. McLean et al. [50] used ReaxFF MD simulations for boron nitride nucleation in CVD, showing oxygen impedes hexagonal ring formation via strong B–O bonds, while H_2O promotes BN bonds and H_2 aids catalytic nanoparticle formation. Analogously in carbon systems, boron doping lowers barriers for sp^2 clustering (0.3–1.0 eV), promoting graphitic domains but risking defects if oxygen coexists, as seen in biomass precursors. This underscores heteroatom dual roles: facilitating (e.g., B-stabilized edges) or inhibiting (e.g., O-crosslinks) transformations, with simulations challenging uniform models by revealing gas-phase vs. surface pathways.

In first stage of carbonization starting with the elimination of volatile species of hetero atoms such as deoxygenation, dehydrogenation, denitrogenation, significant structural ordering often commences in the course of thermal treatment. By releasing these impurities the carbon network turns to be more flexible and thus they can reorganise and hybridise into more staid graphitic structures. To maximise the transformation between the amorphous and graphitic phases of carbon creation and solidify the carbon materials with particular properties useful in energy storage, catalysis, electronics and reinforcing struts, it is crucial to understand and command the part of heteroatoms and impurities [51].

4. Techniques for Inducing Graphitization

It can be accomplished using a variety of physical and chemical methods. The energy input, environmental requirements, spatial control, and scalability of these methods vary. Although thermal annealing is still the most conventional and popular method, developments in catalyst technology, pressure-assisted processing, and irradiation techniques have increased the range of tools available for customising carbon structures. In order to enable graphitic ordering across various precursor types and application contexts, each technique is essential [52].

4.1. Thermal Annealing Processes

These methods are more or less scalable, have different energy input, environmental needs and control over space. Despite the fact that thermal annealing remains the most traditional and widespread technique, improvements in catalyst technologies, pressure-assisted processing, and irradiation techniques have broadened the arsenal of instruments that can be utilised in the modification of carbon structures. To facilitate the process of graphitic ordering in diverse precursor systems and operating environments, both processes are required [53].

Several thermal processing strategies have evolved to optimize the graphitization process. Conventional furnace-based graphitization allows for uniform heating of bulk materials; making it suitable for industrial-scale applications; although it is time- and energy-intensive [54]. Rapid thermal processing offers a faster alternative by exposing carbon samples to short; high-temperature pulses; often used in thin film applications. Laser annealing and Joule heating provide highly localized heating; allowing for selective graphitization with precise spatial resolution [55]. These methods are particularly advantageous in micro- and nano-fabrication; as they permit the patterning of graphitic domains within otherwise amorphous matrices. The final graphitic structure is determined

not only by the maximum temperature achieved but also by the rate of heating and cooling; dwell time at peak temperature; and the overall thermal history of the material [56].

4.2. Catalytic Graphitization

Catalytic graphitization reduces the high energy demands of conventional thermal processing by introducing metal catalysts that promote carbon atom rearrangement at significantly lower temperatures, typically between 700 °C and 1500 °C. Transition metals such as iron, nickel, cobalt, and copper are commonly employed due to their strong interaction with carbon. These metals can be introduced in various forms, including elemental powders, oxides, or metal-organic precursors that decompose into active catalysts during thermal treatment [57].

The underlying mechanisms of catalytic graphitization vary with the catalyst type and process conditions but generally involve three major pathways. In the dissolution-precipitation mechanism, carbon atoms dissolve into the metal at elevated temperatures and later precipitate as graphitic layers upon cooling. Alternatively, metal carbides may form transiently and decompose, releasing graphitic carbon in the process. In surface-mediated reactions, the metal surfaces act as templates, facilitating the alignment of carbon atoms into ordered structures. These catalytic pathways lower the activation energy for graphitization, enabling the formation of graphitic domains under milder conditions [58].

Recent advancements in catalytic graphitization include the development of bimetallic catalysts, which exploit synergistic interactions between different metals to enhance catalytic performance. The use of nanostructured catalysts with high surface area has further improved efficiency and control over graphitic growth. However, challenges remain, particularly regarding the complete removal of residual metal catalysts after processing, as they may affect the purity and performance of the final material. Additionally, heterogeneous distribution of the catalyst can lead to non-uniform graphitization across the carbon matrix [59].

4.3. Pressure-Induced Ordering

Application of pressure during thermal processing has emerged as a powerful strategy to influence the structural evolution of carbon materials. High-pressure treatments can enhance graphitization by promoting densification, reducing interatomic distances, and consequently facilitating the formation of sp^2-bonded networks. Furthermore, pressure can lower the activation energy required for carbon-carbon bond rearrangement, thus accelerating the transformation process. Under directional pressure, graphitic domains may also exhibit preferential alignment, improving anisotropy and enhancing performance in targeted applications [60].

Techniques such as hot isostatic pressing (HIP) combine high temperatures with uniform pressure applied via inert gas media, allowing for isotropic compaction and ordering. Spark plasma sintering (SPS) represents a more advanced approach, applying pulsed electric current alongside pressure to promote rapid heating and graphitization, even in highly refractory carbon systems [61]. Dynamic compression methods, involving the application of extremely high pressures over microsecond timescales (often via impact or explosive forces), have been employed to generate unique graphitic structures with distinctive morphologies and defect patterns [62].

The combination of thermal and pressure treatments offers enhanced flexibility in tuning the microstructure of graphitic carbon. Pressure-assisted graphitization can produce highly ordered structures with improved mechanical and thermal properties, especially useful in composite fabrication, energy storage systems, and thermally conductive components.

4.4. Irradiation Methods

Irradiation-based techniques offer a non-conventional route for inducing graphitization, often enabling precise spatial and temporal control of the process. These methods rely on delivering concentrated energy to the carbon material through electron, ion, laser, or microwave irradiation, leading to localized structural rearrangements and defect generation that can act as nucleation sites for graphitic domains [63,64]. Figure 2 Shows a schematic representation of the microwave irradiation technique for synthesizing decorated activated carbon and scanning electron micrograph of carbon materials.

Electron beam irradiation is particularly effective at the nanoscale, providing energy sufficient to displace carbon atoms and promote rehybridization toward sp^2 bonding. In like manner, ion beam processing also causes localized heating and defects via the impact of the high energy ions thus creating the conditions suitable for graphitic transformation [65]. Laser irradiation utilizes concentrated light of high power to initiate the rapid thermal cycles which in most cases results in the formation of graphitic patterns while the amorphous films or composites are operated with high precision. While microwave irradiation provides a volumetric heating method that can be easily coupled with carbon materials, it further facilitates rapid and energy-efficient graphitization [64,66].

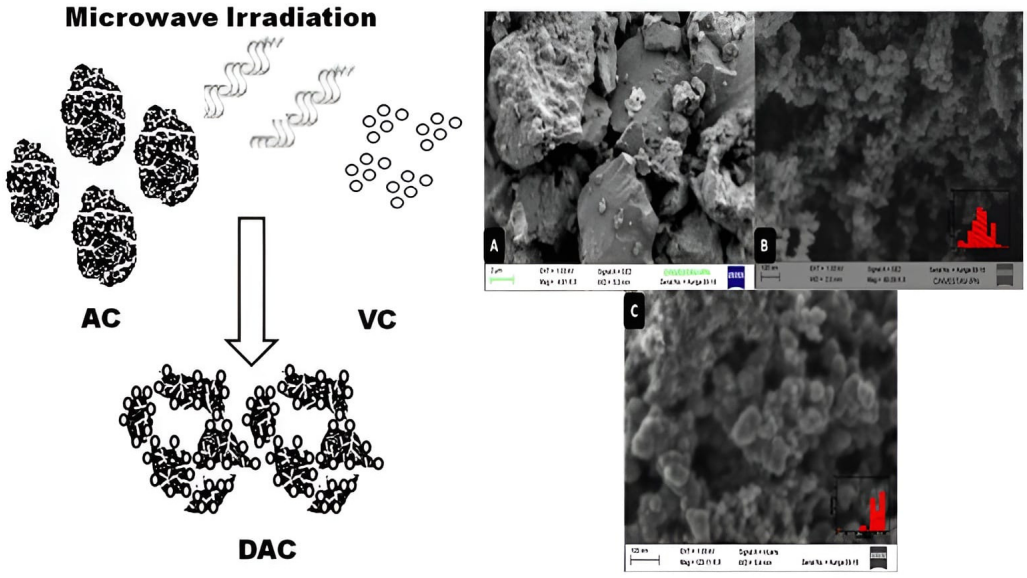

Figure 2. Schematic illustration of the microwave irradiation technique for synthesizing decorated activated carbon (**left**) and scanning electron micrograph of carbon materials (**right**). Reprinted/adapted with permission from Ref. [64]. 2012 Elsevier.

The potential of irradiation methods to target specific parts of a substance to change them into graphite is a major advantage of these methods, which consequently makes them very suitable for microelectronic applications and device manufacturing. Moreover, there is even greater control possible of structural outcome with multiple sequential treatments or with particular mixtures of various forms of irradiation. Recent progressions in in-situ monitoring techniques including electron microscopy and Raman spectroscopy have provided inaccessible insights into the mechanism of transformation and meaningful insight into the mechanisms of the real-time evolution of graphitic domains to irradiation [67].

4.5. Quantitative Comparison of Graphitization Methods

To provide a clearer integration of quantitative data from the literature, we summarize key parameters across the discussed methods. Table 3 outlines typical graphitization temperatures and activation energies, highlighting how catalytic and pressure-assisted approaches reduce energy barriers compared to conventional thermal annealing [11]. For instance, catalytic methods can lower temperatures by 1000–2000 °C through metal-mediated bond reorganization, while pressure-assisted techniques accelerate kinetics at moderate temperatures via activation volume effects [68]. Irradiation methods, such as laser-induced, offer rapid, localized graphitization with variable energies depending on fluence [69].

Table 3. Comparison of Graphitization Temperatures and Activation Energies Across Methods.

Method	Typical Temperature Range (°C)	Activation Energy (kJ/mol)	Notes/Key Influences
Thermal Annealing	2000–3000	120–130 (e.g., 129.2 for boron-free carbons)	High energy; depends on precursor purity and duration; full ordering requires extended annealing [13].
Catalytic Processes	1000–1600	70–90 (e.g., 80.1 with boron or Ni catalysts)	Lowers barriers via metal dissolution-precipitation; effective for biomass precursors [70,71].
Pressure-Assisted Techniques	1000–1500 (with 0.5–8 GPa)	Variable; effective energy reduced by negative activation volumes (−0.7 to −45.7 cm^3/mol)	Accelerates at high P; suitable for rapid recrystallization in subduction-like conditions [68].
Irradiation (e.g., Laser or Electron)	500–1200 (or room temp with high fluence)	30–50 (e.g., ~38.6 from defect annealing)	Photothermal or radiation-induced; fast but localized; lower for powders vs. bulk [69,72].

Table 4 quantifies improvements in electrical/thermal conductivity and mechanical properties, demonstrating enhancements post-graphitization. For example, conductivity can increase 2–5-fold with higher graphitization degrees, while mechanical strength improves due to reduced defects [73,74].

Table 4. Conductivity Improvements and Mechanical Property Changes Post-Graphitization.

Metric	Pre-Graphitization Value	Post-Graphitization Value	Improvement Factor	Method/Notes	Reference
Electrical Conductivity (S/cm)	10–30 (amorphous carbons)	50–100+ (e.g., 27–54 for Ni-catalyzed)	2–5×	Catalytic; increases with crystallinity	[71,75]
Thermal Conductivity (W/m·K)	5–10 (low-graphitized)	15–20+ (e.g., 19.38 for cryptocrystalline)	2–4×	Thermal/Pressure; 2–3× higher in fibers	[73,76]
Young's Modulus (GPa)	10–50 (hard carbons)	50–200+	2–4×	All methods; defect healing enhances	[13,74]
Tensile Strength (MPa)	100–500	500–2000+	1.5–3×	Catalytic/Thermal; increases with carbonization temp	[77]

4.6. Critical Trade-offs in Graphitization Techniques

While the methods discussed offer versatile pathways to induce graphitization, practical implementation requires balancing trade-offs in energy consumption, structural control, process efficiency, and risks like contamination or scalability. Thermal annealing, the benchmark approach, excels in achieving high-purity, well-ordered graphite with excellent structural control (e.g., tunable La/Lc via extended annealing) but demands extreme energy inputs (>2000 °C, often 120–130 kJ/mol activation), leading to high CO_2 emissions and costs [78,79]. Catalytic processes mitigate this by lowering temperatures (1000–1600 °C) and barriers (70–90 kJ/mol with Fe/Ni), enhancing efficiency for biomass precursors, but introduce contamination risks from metal residues, necessitating acid washing that adds environmental burdens (e.g., Fe removal efficiency ~97% but wastewater generation) [80]. Pressure-assisted techniques provide rapid kinetics at moderate conditions (1000–1500 °C with 0.5–8 GPa), improving structural uniformity in subduction-like scenarios, yet require specialized equipment, limiting scalability and raising safety concerns [81]. Irradiation methods (e.g., laser or electron) enable low-energy, localized graphitization (500–1200 °C, 30–50 kJ/mol), ideal for nanostructures, but suffer from non-uniformity and high initial setup costs, with efficiency tied to fluence control [82,83].

Sustainability trends favor catalytic and irradiation for reduced energy (e.g., 50% savings vs. thermal) and greener precursors like biomass, though trade-offs persist: catalytic efficiency (e.g., 2–3× faster ordering) vs. impurity removal (e.g., Fe/Co residues impacting purity <99.95% for batteries) [84]. Overall, hybrid approaches (e.g., catalytic-pressure) may optimize these, but require case-specific evaluation—thermal for high-purity bulk graphite, catalytic for scalable, low-cost nanostructures. Table 5 summarizes key trade-offs, emphasizing the need for integrated metrics like energy per kg graphite produced (~10–20 MJ/kg thermal vs. 5–10 MJ/kg catalytic) to advance high-impact applications [79].

Table 5. Trade-offs in Graphitization Techniques.

Method	Energy Consumption	Structural Control	Efficiency	Contamination Risks	Pros	Cons
Thermal Annealing	High (2000–3000 °C; 120–130 kJ/mol) [73,85]	Excellent (high purity, tunable domains) [86]	Moderate (slow kinetics) [87]	Low (no additives) [73]	Reliable for bulk; high ordering [88]	Energy-intensive; high emissions; costly [89]
Catalytic Processes	Moderate (1000–1600 °C; 70–90 kJ/mol) [90]	Good (catalyst-dependent; e.g., Fe for nanotubes) [71]	High (2–3x faster; lowers barriers) [91]	High (metal residues; need removal ~97% efficient) [80,92]	Energy savings 30–50%; scalable for biomass [92]	Post-processing wastewater; purity issues for batteries [84]
Pressure-Assisted	Moderate (1000–1500 °C + pressure) Chen et al., 2018 [93]	Very good (uniform recrystallization) [13]	High (accelerated by volume effects) Gentile et al., 2024 [94]	Low-moderate (if no catalysts) Zhao et al., 2009 [95]	Rapid; suits high-density	Equipment costs; safety risks; limited scale Oluwole et al., 2025 [96]
Irradiation (Laser/Electron)	Low (500–1200 °C; 30–50 kJ/mol) [83]	Variable (localized; fluence-dependent) [97]	Very high (fast, seconds-minutes) [98]	Low (non-contact) [99]	Precise, low-energy; nanostructures [100]	Non-uniform; high setup; not for bulk [101–103]

4.7. Advanced Characterization Techniques for Probing Graphitization Dynamics

While graphitization methods are well-established, advanced characterization tools like in-situ TEM, Raman spectroscopy, and XRD uniquely enable real-time, multi-scale insights into the process, advancing our understanding of kinetics (e.g., transformation rates), heterogeneity (e.g., spatial variations in ordering), and intermediate states (e.g.,

metastable phases). In-situ TEM provides atomic-resolution visualization of dynamic transformations, capturing heterogeneity in domain growth and defect evolution during heating or catalysis. For instance, it reveals nickel-catalyzed graphitization kinetics in amorphous carbon films, showing carbide intermediates forming at ~500–700 °C with domain expansion rates of ~1–5 nm/s, highlighting localized heterogeneity overlooked in bulk methods [104]. Similarly, in-situ TEM tracks free-standing graphene growth from nanocrystalline precursors, identifying intermediate turbostratic states and stress-induced alignment, with kinetic barriers reduced under electron beam effects [105]. Its sub-second temporal resolution (~ms) excels for operando studies in heterogeneous catalysis, exposing phase transitions in real-time [106].

Raman spectroscopy offers non-destructive, vibrational insights into chemical bonding and disorder, ideal for quantifying kinetics and heterogeneity via band parameters (e.g., D/G ratio for defects). It models kerogen-to-graphite transitions, deriving activation energies (~200–300 kJ/mol) from spectral evolution, revealing heterogeneous maturation paths in natural carbons [107]. In coal-derived chars, Raman mapping uncovers structural heterogeneity, with peak fitting showing varied graphitization degrees (sp^2 clusters vs. amorphous regions) and kinetic rates influenced by pyrolysis temperatures [108]. It also probes laser-heated carbon blacks' graphitization kinetics, tracking intermediate states like partial ordering with D-band narrowing over seconds [109]. Raman's micron-scale resolution complements bulk techniques, highlighting thermal history effects on heterogeneity.

XRD quantifies crystalline order through diffraction patterns, excels in tracking intermediate states via lattice parameters (e.g., d002 spacing decreasing from ~0.35 nm amorphous to 0.335 nm graphite). It assesses graphitization degrees in heterogeneous materials, correlating with kinetics under pressure (e.g., rapid recrystallization at 0.5–8 GPa, reducing times from hours to seconds [68]. In iron-catalyzed hard carbons, XRD reveals evolutionary intermediates like metal carbides, with graphitization indices increasing heterogeneously across samples [39]. It also evaluates structural heterogeneity in nuclear graphites, linking microcrystalline variations to performance (e.g., IG-110 vs. NBG-18 differing by ~10% crystallization) [110]. XRD's ensemble averaging provides statistical kinetics, complementing TEM's local views.

These tools synergize for comprehensive analysis: e.g., in-situ TEM-Raman hybrids capture atomic heterogeneity and bonding changes simultaneously. Table 6 outlines their unique advancements, underscoring their role in resolving long-standing debates on uniform vs. heterogeneous pathways.

Table 6. Unique Contributions of Characterization Tools to Graphitization Understanding.

Tool	Key Insights into Kinetics	Key Insights into Heterogeneity	Key Insights into Intermediate States	Resolution/ Advantages	Limitations	Reference Examples
In-situ TEM	Real-time domain growth rates (~1–5 nm/s); activation under catalysis	Localized variations in ordering and defects	Carbide/turbostratic phases during transformation	Atomic (~Å), temporal (~ms)	Beam-induced artifacts; small sample	[104,105]
Raman Spectroscopy	Activation energies (~200–300 kJ/mol); spectral evolution rates	Micron-scale mapping of disorder (D/G ratios)	Partial ordering transitions (band narrowing)	Molecular (~cm^{-1}), non-destructive	Surface-sensitive; peak overlap	[107–109]
XRD	Pressure-accelerated rates (s vs. h); index evolution	Ensemble heterogeneity in crystallization (~10% variations)	Lattice spacing shifts identifying carbides	Crystalline (~nm), bulk statistics	Averaged data; less dynamic	[39,68,110]

4.8. Sustainability Challenges and Strategies in Graphitization

Traditional graphitization techniques, particularly thermal annealing at >2000 °C, pose significant sustainability challenges due to high energy demands (10–20 MJ/kg graphite) and associated CO_2 emissions (5–10 kg/kg from fossil fuel heating), exacerbating climate impacts and limiting scalability for mass production [13,54]. These processes often rely on non-renewable precursors like petroleum coke, contributing to resource depletion and environmental pollution from volatile emissions. Catalytic methods, while lowering temperatures, introduce scalability issues (e.g., catalyst recovery) and potential contamination from metals like Ni or Fe, which require energy-intensive purification [111]. Pressure-assisted and irradiation approaches offer partial relief but face barriers in equipment costs and energy inefficiency for large-scale deployment.

To mitigate these, emerging strategies emphasize low-energy, green alternatives. Microwave-assisted graphitization enables rapid heating (seconds to minutes) at 500–1000 °C via selective dielectric absorption, reducing energy by 50–80% and emissions through targeted heating, as demonstrated in coal-derived graphene synthesis [112,113]. Green catalysts, such as boron or natural iron oxides from biomass, lower activation barriers without toxic residues, facilitating graphitization at <1500 °C and promoting circularity (e.g., using waste biomass

as both precursor and catalyst source) [114,115]. Biomass-derived precursors (e.g., coconut shell or sugarcane bagasse) enable sustainable feedstocks, converting low-value waste into high-graphitization carbons with yields >50% and reduced emissions (e.g., CO_2-neutral via bio-carbon) [116,117]. Hybrid approaches, like microwave-catalytic with green additives, further enhance scalability for applications in batteries and composites, potentially cutting costs by 30–50 [89]. Future prospects include electrochemical graphitization for room-temperature processes, urging integrated life-cycle assessments to balance performance and eco-impact. Table 7 compares conventional and sustainable graphitization methods, highlighting differences in temperature, energy use, CO_2 emissions, scalability and key strategies. Sustainable approaches, such as green catalytic and biomass-derived hybrid methods, offer lower emissions, energy efficiency, and better circular economy compatibility.

Table 7. Comparison of Conventional vs. Sustainable Graphitization Methods.

Method Type	Temperature (°C)	Energy (MJ/kg)	CO_2 Emissions (kg/kg)	Scalability	Key Strategies/Notes	Reference
Conventional Thermal	2000–3000	10–20	5–10	Moderate (bulk, energy-intensive)	High purity but unsustainable	[13]
Catalytic (Traditional)	1000–1600	5–10	2–5	High (with recovery)	Metal residues; green alternatives needed	[111]
Microwave-Assisted	500–1000	2–5	1–2	High (rapid, localized)	Low-energy; biomass compatible	[112,113]
Green Catalytic (Boron/Biomass)	800–1500	3–7	<2 (renewable)	Moderate-High	Low-toxicity; circular economy	[114,115]
Biomass-Derived Hybrid	900–1200	4–8	0–1 (CO_2-neutral)	High (waste utilization)	Scalable for green graphite industry	[116,117]

5. Characterization of Graphitization Processes

This review provides a comprehensive overview of the structural transformation from amorphous carbon—particularly in graphitizable soft carbons—to ordered graphitic crystalline planes, emphasizing the underlying mechanisms, advanced characterization techniques, and diverse applications. The complexity of this transformation and the huge number of possible structural states require the employment of a variety of advanced analytical tools in order to study microstructural, chemical and functional changes taking place during and after graphitisation. Besides giving an insight into the processes during the transformation, the practices provide essential assistance in optimising synthesis and tailoring the particle properties to specific applications.

5.1. Structural Characterization Techniques

Structural transformations that occur in connection with the process of graphitisation are commonly traced and studied by a combination of diffraction, spectroscopic, and microscopic methods. The X-ray diffraction (XRD) is critical because it provides quantitative data regarding crystalline in nature of carbon materials. This amorphous-ordered graphitic phase transformation is evident in the shift of the XRD pattern in response to a shift of poorly resolved and angular maximum to sharp well-formed reflections. Application of derived parameters in order to determine the level of graphitisation is based on stacking height (Lc), in-plane crystallite size (La) and inter-layer d spacing (0 0 2) [118].

Due to its extreme sensitivity to structural arrangement as well as carbon bonding, other important tool is Raman spectroscopy (see Figure 3). The presence and progression of G band (~1580 cm^{-1}), D band (~1350 cm^{-1}) and 2D (G) bond (~2700 cm^{-1}) elaborate on defect density, layer stacking, and sp^2 bonding environment. One of the typically used measures of disorder and progression of graphitisation is D to G band intensity ratio (ID/IG). Figure 3 show Raman spectra of the synthesized green carbon with I_D/I_G [19,119].

Transmission electron microscopy (TEM) (high-resolution TEM and selected area electron diffraction (SAED)) can also be directly used to provide information about local crystallinity, domain orientation and stacking of graphene layers [120]. Electron energy loss spectroscopy (EELS) can also be used to quantitatively measure the ratio of sp^2 to sp^3 hybridisation, and thus is useful in mapping the electronic and bonding chemistry within the carbon network [121]. X-ray photoelectron spectroscopy (XPS) complements knowledge of surface chemistry and bond state by measuring the distribution and types of carbon, heteroatom, etc. in the material [122].

Recent advances in in-situ characterisation make it possible to monitor the graphitisation process under near real-world conditions. These methods are providing a more thorough understanding of graphitisation mechanisms by illuminating spatial heterogeneities within samples, transformation kinetics, and transient intermediate phases.

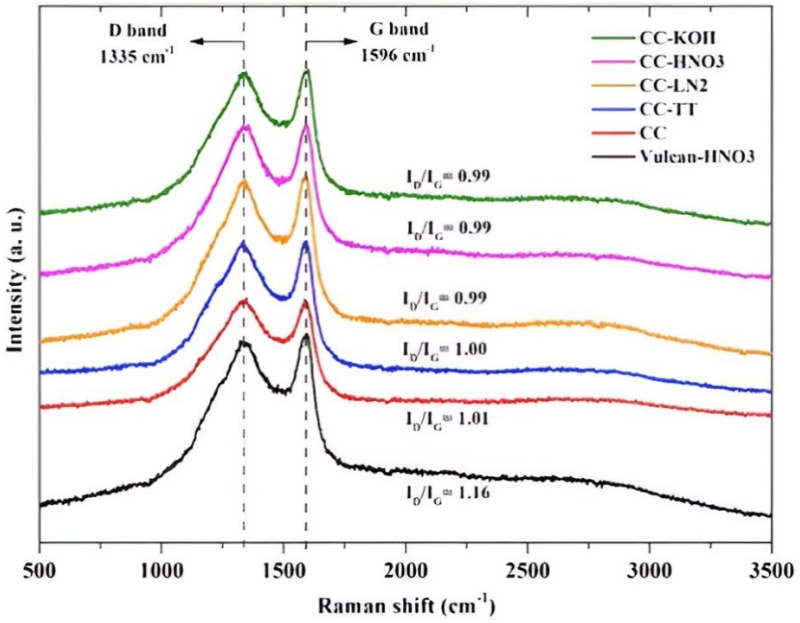

Figure 3. Raman spectra of the synthesized green carbon with I_D/I_G. Reprinted/adapted with permission from Ref. [19]. 2015 Elsevier.

5.2. Property Evolution during Graphitization

As structural ordering progresses during graphitization, the physical and chemical properties of carbon materials undergo significant changes. One of the most noticeable transformations is in electrical conductivity. The formation of extended π-conjugated networks in graphitic structures allows for band-like electron transport, leading to conductivity increases by several orders of magnitude compared to the disordered, hopping-dominated conduction typical of amorphous carbon [123].

Thermal properties also improve significantly during graphitization. Enhanced structural order reduces phonon scattering, thereby increasing thermal conductivity, particularly in the plane of the graphitic layers. Specific heat capacity also gradually approaches the theoretical values for graphite as the material becomes more crystalline [73].

Mechanical properties evolve in more complex ways. While in-plane stiffness and Young's modulus generally increase due to the formation of strong sp^2 carbon networks, the weak van der Waals forces between graphitic layers can limit the material's resistance to shear and delamination. These effects create a balance between enhanced rigidity and increased brittleness [124].

Surface and chemical properties change as well, with graphitized surfaces typically exhibiting lower reactivity, reduced surface energy, and altered wettability compared to their amorphous counterparts. These changes are particularly important for applications such as catalysis, sensing, and composite reinforcement, where surface characteristics dictate interfacial behavior. Monitoring these property changes not only serves to evaluate the quality of graphitization but also helps establish correlations between processing parameters, structural evolution, and end-use performance [125].

5.3. In-Situ Monitoring of Transformation Processes

Real-time analysis of structural, chemical, and functional changes during transformation is now possible thanks to the development of in-situ monitoring tools, which has completely changed the study of graphitisation. With an in situ TEM equipped with heating stages or environmental cells, researchers get to see with combinations of atomic resolution rearrangement of carbon atoms, and the formation of graphitic domains. This method throws more light on resolving dynamics of domain growth, defect migration, and nucleation sites [126].

Such observations are endorsed by in-situ Raman spectroscopy that tracks alterations in disorder and graphitic order as evaluated by spectral evolution through heating cycles. The passage between the transition thresholds as well as intermediate states may be observed in graphitisation due to the continuous observation of the peak positions, intensities and full-width at half-maximum (FWHM) [127]. In-situ X-ray diffraction represents a powerful method of monitoring interlayer spacing and crystallite size and preferred orientation variations in response to atmospheric and temperature variations. The technique can be helpful in charting the dynamic structure rearrangement and crystalline growth kinetics. Besides, in-situ electrical measurements provide the dynamic

analysis of conductivity and percolation behaviour as the conductive graphitic networks emerge. Such measurements have found useful application in having an understanding of the development of electronic pathways of the porous and composite systems [128].

The combination of several in-situ techniques provides a comprehensive picture of the process of graphitisation because, as it turns out, transformation often takes place in a heterogeneous fashion with different spatial regions undergoing different structural transformations. These advanced monitoring functions are vital in the development of predictive graphs and individualised processing strategies of the next-generation graphitic materials.

5.4. Applications of Graphitized Carbon Materials

Controlled graphitization transforms amorphous carbon into materials with tailored properties, critically impacting performance in energy storage, electronics, composites, and sensing. Here, we compare how graphitization degree (DoG) affects key metrics, drawing on recent quantitative data to highlight optimizations and limitations.

In lithium-ion batteries (LIBs), higher DoG improves electrical conductivity and lithium intercalation, boosting specific capacity and rate performance, but excessive graphitization can reduce active sites due to fewer defects. For coal-derived anodes, DoG of ~80–90% yields specific capacities of 300–350 mAh/g, compared to <200 mAh/g for low-DoG (~50%) materials, with conductivity rising from ~10 S/cm to >50 S/cm [73]. Bio-graphite with 89.28% DoG achieves ~320 mAh/g, outperforming commercial graphite in stability but requiring optimization to mitigate volume expansion [129]. Critically, DoG >90% enhances fast-charging (e.g., 80% capacity retention at 5C) but increases costs via high-temperature processing.

For supercapacitors, elevated DoG enhances conductivity and capacitance via better electron transport and surface area retention, though over-graphitization may collapse pores, limiting ion accessibility. Boron-catalyzed graphitized biochar (DoG ~85%) delivers 144 F/g at 1 A/g, versus 87 F/g for lower-DoG (~60%) counterparts, with conductivity improved by ~2–3× [116]. Laser-induced graphene achieves ~200 F/g with high DoG, but heterogeneity reduces cycle life (<90% retention after 10,000 cycles) compared to moderate-DoG materials [130]. Optimal DoG (~70–80%) balances capacitance and durability for high-power applications.

In composites, higher DoG strengthens thermal/electrical conductivity but can degrade mechanical properties via crystallite growth-induced defects. Carbon fiber composites at 1600 °C (high DoG) show flexural strength of 364 MPa (vs. 300 MPa untreated), but tensile strength drops to 2.98 GPa at 1200 °C due to stress concentration [131]. Graphene-reinforced composites with DoG ~90% exhibit Young's modulus up to 200 GPa, 2–4× untreated, yet brittleness limits impact resistance [132]. Moderate DoG (~70%) optimizes toughness for aerospace uses.

For sensors, increased DoG boosts conductivity and sensitivity through efficient charge transfer, but excessive ordering reduces active sites for analyte binding. Graphene-based pressure sensors with optimized DoG (~80–90%) achieve sensitivity of 232.5 kPa^{-1} (0–0.2 kPa range) and conductivity ~10^3 S/cm, far surpassing low-DoG (~50%) at <50 kPa^{-1} [133]. Ozonated expanded graphite (modulating effective DoG) shows CO sensitivity up to 31.07% with resistance drops to 0.157 kΩ, but over-processing lowers it to 8.90% [134]. High DoG favors fast response (<50 ms) but trades off selectivity in gas sensors. Table 8 shows that a higher degree of graphitization (DoG) enhances performance metrics such as capacity, conductivity, strength, and sensor sensitivity across batteries, supercapacitors, composites, and sensors, but often at the expense of cost, brittleness, or selectivity.

Table 8. Impact of Graphitization Degree on Performance Metrics.

Application	Low DoG (~50–60%)	High DoG (~80–90%)	Key Trade-off	Reference
Batteries (Specific Capacity, mAh/g)	<200; Conductivity ~10 S/cm	300–350; ~50 S/cm	Higher capacity vs. cost/expansion	[73,129]
Supercapacitors (Capacitance, F/g)	87; Lower conductivity	144; 2–3× higher	Capacitance vs. pore collapse	[116,130]
Composites (Strength/Modulus, MPa/GPa)	Flexural 300; Modulus ~50	Flexural 364; Modulus 200	Strength vs. brittleness	[131,132]
Sensors (Sensitivity)	<50 kPa^{-1}/ 9.66% (CO)	232.5 kPa^{-1}/ 31.07% (CO)	Sensitivity vs. selectivity	[133,134]

6. Applications of Controlled Graphitization

The controlled graphitisation of amorphous carbon has led to a large number of high-tech applications; this conversion changes the amorphous carbon into the graphitic forms. It is also possible to adjust the characteristics of carbon based materials to meet specific functional criteria through manipulating the extent of ordering, spatial arrangement of graphitic domains, and structural parameters. This part focuses on the benefits of these transformations at various areas, including energy storage and the next generation quantum technologies.

6.1. Energy Applications

Due to its outstanding conductivity, stability, and open porosity that can be replicaed, graphitised carbon materials have become fundamental in the energy storage sector. An example is the graphitised carbon, which is a typical anode material in the lithium ion battery (LIBs), and its high degree of ordering gives rise to the potential efficiency of transferring electrons and structural stability during thousands of repetitive charge-discharge cycles [3,135,136]. The partially graphitized carbons come out to be the best of both the worlds i.e., they contain the properties of ordered domains due to which they can transport the ions in less time and the disordered regions as well which enhances the storage capacity of lithium [137]. Similarly, in supercapacitors, the controlled graphitization of carbon helps optimize surface area, pore size distribution, and conductivity, all of which are critical for achieving high capacitance and rapid charge-discharge performance [138]. Graphitized structures also hold promise for hydrogen storage, where precisely tailored pores and surface chemistries can facilitate effective adsorption, although achieving practical storage capacities remains a challenge [139]. In sodium- and potassium-ion batteries, partial graphitization proves even more beneficial than complete ordering, as the larger ionic radii of these elements favor structures that maintain both flexibility and accessibility [140]. Recent research trends emphasize the fabrication of hierarchical carbon materials that integrate multiple levels of graphitization to maximize ion storage, conductivity, and mechanical stability simultaneously.

Carbon-based composite materials are increasingly utilized in microbial fuel cells (MFCs) as membranes and in proton exchange membrane (PEM) fuel cells as catalyst supports, advancing sustainable energy technologies. In MFCs, composites blending natural clays with activated carbons such as bone char, coconut shell, or bituminous types, often modified with sulfuric acid serve as cost-effective proton exchange membranes, enhancing proton diffusion coefficients (up to 0.21 × 10^{-5} cm^2/s), oxygen mass transfer, and overall power density while demonstrating practical applications like powering LEDs and clocks [3]. Meanwhile, in PEM fuel cells, bio-derived carbons like those from camote (sweet potato) act as efficient catalyst supports for platinum nanoparticles, providing high surface area and conductivity comparable to commercial Vulcan carbon, thereby improving oxygen reduction reaction kinetics and reducing reliance on expensive materials for cleaner energy production [19]. Figure 4 shows schematic of preparation of mesoporous soft carbon from bone char, coconut shell activated carbon and bituminous activated carbon and natural clay and particle size of the Pt catalysts supported on various carbon materials determined from the particle count of the HR-TEM micrographs; in addition Proton Exchange Membrane Fuel Cells (PEMFC) directly produce electrical energy by converting the chemical energy stored in fuels, such as hydrogen and methanol with a low environmental impact on the other hand are show well-defined nano-separated hydrophilic and hydrophobic phases and percolated nanodomains for Nafion [141].

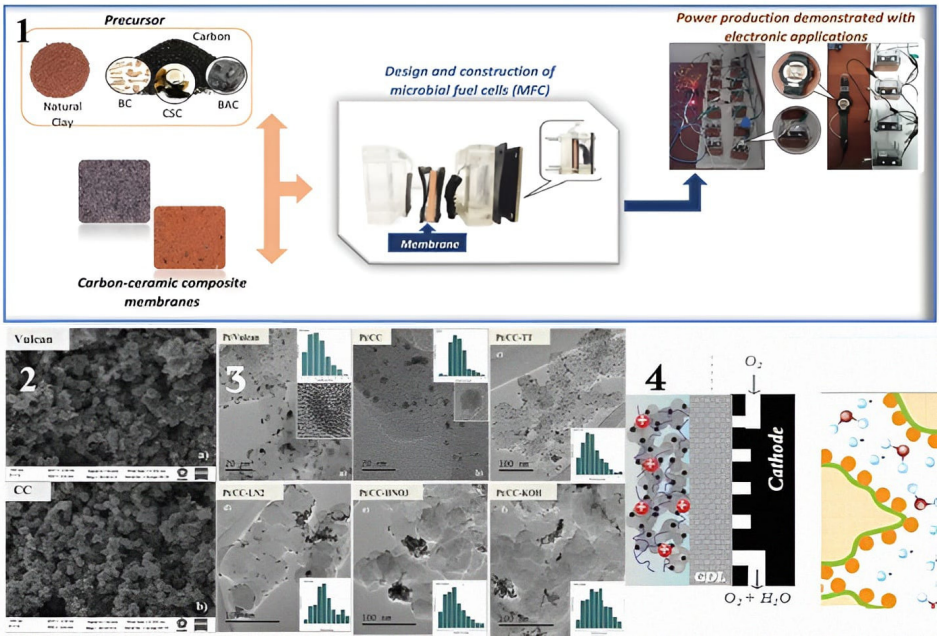

Figure 4. (**1**) Schematic illustration of preparation of mesoporous soft carbon; (**2**) SEM micrographs for Vulcan Carbon and Camphor carbon (CC); (**3**) HRTEM micrograph with size distribution for Pt/C catalyst; Reprinted/adapted with permission from Ref. [3,19]. 2023, 2015 Elsevier. (**4**) Schematic representation of a Proton Exchange Membrane Fuel Cells and e.g., Nafion and its chemical structure and morphology. Reprinted/adapted with permission from Ref. [141], 2025.

6.2. Electronic and Sensor Applications

Graphitized carbon plays a critical role in electronic and sensor technologies due to its highly tunable electrical characteristics. For transparent conductive films used in flexible displays and electronics, partially graphitized carbon layers offer an ideal balance between optical transparency and electrical conductivity [142]. Chemical sensors benefit from the introduction of graphitic domains within amorphous matrices, which enhances analyte sensitivity by improving both adsorption efficiency and electron [136,143]. This principle is also applied in electrochemical sensors, where the interplay between reactive graphitic edge sites and conductive basal planes contributes to superior detection capabilities. In applications such as electromagnetic interference (EMI) shielding, the electrical properties resulting from graphitization can be engineered to absorb or reflect unwanted radiation, making carbon-based composites useful in aerospace and consumer electronics [144]. Figure 5 shows a summarized schematic of various surface modifications carbon based for a catecholamine detection in biomedical applications to diagnose several brain diseases by rapidly detecting neurotransmitters and biomolecules related to the nervous system [145]. Field emission devices also exploit the sharp, conductive tips formed during localized graphitization, which serve as efficient electron sources. The development of spatially selective graphitization techniques such as laser writing and electron beam exposure has enabled precise patterning of carbon-based devices with region-specific functionalities, advancing the integration of graphitized carbon in modern electronics [146].

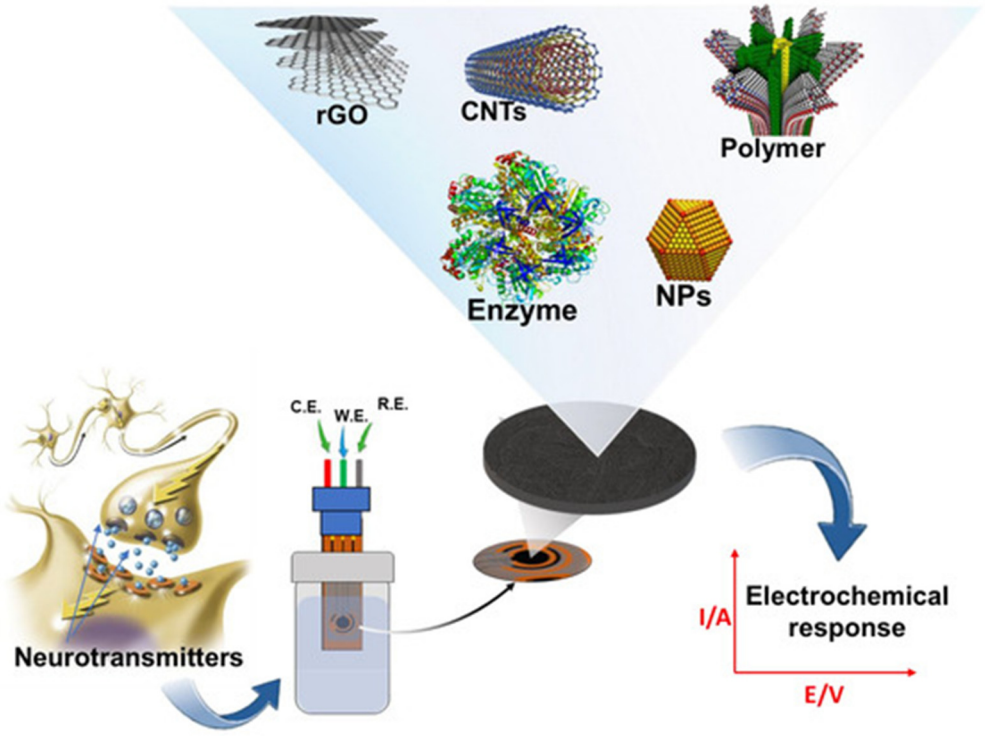

Figure 5. Simplified diagram showing electrochemical sensors/biosensors [145].

6.3. Structural and Composite Materials

The mechanical properties of carbon materials undergo significant changes with graphitization, enabling their use in high-performance structural and composite applications [136]. In carbon fiber production, controlled graphitization enhances tensile strength, stiffness, and thermal stability, qualities that are highly valued in aerospace, automotive, and defense industries [147]. Partially graphitized carbon materials also function as self-lubricating components, particularly under extreme mechanical or thermal conditions, where they offer an optimal combination of wear resistance and lubricity [148]. Their high thermal conductivity makes them effective materials for heat dissipation in electronic systems, where managing thermal loads is essential for performance and longevity. Additionally, biomedical applications benefit from graphitized carbon structures that combine mechanical robustness with biocompatibility, making them suitable for orthopedic implants and dental prosthetics [149]. Emerging innovations in this domain involve the creation of gradient-graphitized materials, in which spatial variations in graphitic ordering are introduced to meet complex mechanical or thermal performance requirements within a single component or device [150].

6.4. Emerging Applications

Beyond conventional uses, controlled graphitization is enabling a new generation of cutting-edge technologies. In catalysis, partially graphitized carbon materials serve as ideal supports for metal nanoparticles in fuel cells and electrochemical reactors, offering high conductivity, tunable surface functionality, and structural stability [3,136,151]. Environmental remediation is another promising field, where the adsorption capacity and chemical selectivity of carbon materials can be precisely tuned through graphitization to target specific pollutants in air or water [152]. In thermal energy harvesting, the creation of spatially varied graphitic structures allows for thermoelectric effects, where temperature gradients are converted into electrical energy. Neuromorphic computing also benefits from the mixed amorphous-graphitic architecture, which mimics synaptic behavior through memristive properties, offering low-power, brain-like computing capabilities [153].

Various techniques have been developed to achieve this transformation, each characterized by distinct reaction conditions, temperatures, and applications. This discussion synthesizes key parameters from comparative analyses, highlighting thermal annealing processes, catalytic graphitization, pressure-induced ordering, and irradiation methods (Table 9).

Thermal annealing processes represent foundational approaches to graphitization, relying on high-temperature treatments to reorganize carbon atoms into sp^2-bonded layers. Conventional furnace-based graphitization typically requires temperatures above 2000 °C, often exceeding 2500 °C, with prolonged heating durations to facilitate atomic diffusion and crystallization. This method is well-suited for industrial-scale production due to its scalability and reliability in yielding bulk graphitic materials [5,53,125]. In contrast, rapid thermal processing employs short, intense high-temperature pulses, offering a faster alternative ideal for thin-film applications where minimizing processing time is crucial [53]. Advanced variants like laser annealing and Joule heating provide highly localized heating, enabling selective graphitization with exceptional spatial resolution. These are particularly advantageous in micro- and nano-fabrication, allowing precise patterning of graphitic domains within amorphous carbon matrices for devices such as sensors and electronics [53,55].

Catalytic graphitization lowers the energy barrier by incorporating metal catalysts, operating at moderate temperatures between 700 °C and 1500 °C. Catalysts such as iron, nickel, cobalt, and copper facilitate the dissolution and precipitation of carbon, promoting ordered growth while reducing the high energy demands of purely thermal methods. This technique is widely applied in producing graphene and carbon nanotubes from amorphous precursors, enhancing long-range structural order and efficiency. Innovations like nanostructured or bimetallic catalysts further improve control over graphitic growth, making it suitable for scalable nanomaterial synthesis [9,28,57,58].

Pressure-induced ordering integrates mechanical forces with thermal processing to accelerate graphitization. Methods like hot isostatic pressing (HIP) apply uniform high pressure at elevated temperatures, while spark plasma sintering (SPS) uses pulsed electric currents for rapid heating under pressure. Dynamic compression techniques employ extreme pressures via impacts or explosives over microseconds. These approaches promote densification, reduce interatomic distances, and lower activation energy, fostering sp^2 network formation and domain alignment. Resulting materials exhibit enhanced anisotropy, mechanical strength, and thermal conductivity, finding applications in composites, energy storage (e.g., batteries), and heat-dissipating components [60–62].

Irradiation methods deliver focused energy through electron, ion, laser, or microwave beams, enabling precise control over graphitization. Electron and ion beams induce nanoscale defects as nucleation sites, while laser and microwave irradiation cause rapid, volumetric heating. Operating under ambient or moderate conditions, these techniques offer spatial and temporal precision, making them ideal for microelectronics and device fabrication. Sequential or hybrid irradiations enhance structural outcomes, supporting energy-efficient processes with minimal thermal damage [63,65,66].

In summary, the choice of graphitization technique hinges on balancing temperature requirements, processing speed, and application needs. While thermal methods excel in bulk production, catalytic and pressure-based approaches reduce energy use, and irradiation offers precision for advanced nanotechnology. Future advancements may integrate these for hybrid systems, optimizing efficiency across diverse fields.

Furthermore, graphitized carbon materials are being explored in quantum information science, where isolated structural defects within graphitic domains can serve as stable quantum bits (qubits) for sensing and data processing applications [154]. These frontier applications are driven by growing control over nanoscale graphitization processes, as well as a deeper understanding of how structural transformations influence the physical, chemical, and electronic behavior of carbon materials [155].

Table 9. Comparative Summary of Different Graphitisation Processes, Their Reaction Conditions, and Corresponding Applications.

Technique	Reaction Conditions/Temperature	Respective Applications	References
Thermal Annealing Processes	Conventional furnace-based graphitization: High temperatures, often above 2000 °C, even over 2500 °C, and long heating times.	Suitable for industrial-scale applications.	[5,53,125]
	Rapid thermal processing: Short, high-temperature pulses.	Faster alternative for thin film applications.	[53]
	Laser annealing and Joule heating: Highly localized heating.	Enables selective graphitization with precise spatial resolution, advantageous in micro- and nano-fabrication, allowing patterning of graphitic domains within amorphous matrices.	[53,55]
Catalytic Graphitization	Lower temperatures, typically between 700 °C and 1500 °C, using metal catalysts like iron, nickel, cobalt, and copper.	Reduces high energy demands of conventional thermal processing. Applied to the production of graphene and carbon nanotubes from amorphous carbon materials. Enhances long-range order development. Improved efficiency and control over graphitic growth with nanostructured and bimetallic catalysts.	[9,28,57,58]
Pressure-Induced Ordering	Application of pressure during thermal processing. Techniques include hot isostatic pressing (HIP) (high temperatures with uniform pressure) and spark plasma sintering (SPS) (pulsed electric current alongside pressure for rapid heating). Dynamic compression methods (extremely high pressures over microsecond timescales via impact or explosive forces).	Enhances graphitization by promoting densification, reducing interatomic distances, and facilitating sp^2-bonded network formation. Lowers activation energy and accelerates transformation. Can induce preferential alignment of graphitic domains, improving anisotropy. Produces highly ordered structures with improved mechanical and thermal properties, useful in composite fabrication, energy storage systems, and thermally conductive components.	[60–62]
Irradiation Methods	Delivery of concentrated energy through electron, ion, laser, or microwave irradiation. Electron beam irradiation effective at nanoscale. Ion beam processing causes localized heating and defects. Laser irradiation initiates rapid thermal cycles. Microwave irradiation provides volumetric heating.	Enables precise spatial and temporal control of the process. Leads to localized structural rearrangements and defect generation that act as nucleation sites for graphitic domains. Very suitable for microelectronic applications and device manufacturing. Allows rapid and energy-efficient graphitization. Offers greater control over structural outcome with sequential or mixed irradiation treatments.	[63,65,66]

7. Challenges and Future Perspectives

The science and technology of carbon graphitization have advanced impressively, enabling applications ranging from electronics to energy storage. Yet several critical challenges remain. Conventional graphitization demands extremely high temperatures (often over 2500 °C) and long heating times, resulting in high energy consumption and carbon emissions that limit sustainability and scalability [125]. Moreover, achieving precise spatial control over the degree of graphitization at micro- and nanoscales remains difficult, hindering the production of integrated devices with region-specific properties. Another key limitation lies in property trade-offs: while increased graphitization improves electrical conductivity, it often reduces surface area and chemical reactivity needed for catalysis or energy storage [156]. Addressing these competing demands requires sophisticated process control and optimization strategies. Environmental concerns further complicate the landscape, as many high-temperature and catalytic processes produce toxic byproducts or consume scarce resources [157]. Additionally, the atomic-scale mechanisms underlying graphitization, especially with bio-derived or complex precursors, remain poorly understood, limiting rational design of new processes [158]. To overcome these challenges, interdisciplinary research is focusing on low-temperature graphitization methods such as catalytic, electrochemical, and microwave-assisted approaches, which reduce energy use and enable new substrates [64,67]). Advanced techniques like laser-based graphitization offer spatial programmability, while machine learning aids in optimizing parameters and predicting outcomes [159]. In-situ characterization tools are revealing real-time transformation dynamics, deepening understanding. Sustainability strategies emphasize renewable carbon sources, green catalysis, energy-efficient furnaces, and life cycle assessments, ensuring environmental impacts are minimized [160]. Circular economy concepts, such as recycling and repurposing graphitized materials, are also gaining traction, reinforcing the push toward cleaner, more sustainable carbon technologies.

8. Conclusions

The transformation from amorphous carbon to ordered graphitic structures represents both a fascinating fundamental science challenge and an enabling technology for numerous applications. This review has examined the current understanding of transformation mechanisms, the diverse techniques for inducing and controlling graphitization, characterization approaches, and the expanding landscape of applications. Recent years have witnessed significant advances in our ability to control carbon crystallization processes at multiple length scales, enabling increasingly sophisticated carbon materials with tailored properties. The integration of in-situ characterization techniques with advanced processing methods has substantially deepened our understanding of the complex pathways through which disordered carbon structures transform into ordered graphitic arrangements. Looking forward, the field appears poised for continued innovation through the convergence of several trends: more energy-efficient processing approaches, spatially controlled graphitization, data-driven optimization, and sustainability-focused research directions. These developments promise to expand the application space for graphitized carbon materials while addressing existing limitations related to energy intensity, process control, and environmental impact. As our fundamental understanding and technological capabilities continue to advance, the controlled transformation from amorphous to graphitic carbon will likely remain an active and fruitful research area with substantial technological impact across diverse sectors including energy, electronics, structural materials, and emerging technologies.

Author Contributions

A M.-G: writing—original draft preparation, writing—reviewing and editing, M.K.S.: writing—original draft preparation, writing—reviewing and editing, I.A.A.: data curation, W.A.: data curation, supervision, A.T.: data curation, supervision S.-K.K.: conceptualization, methodology, writing—original draft preparation. All authors have read and agreed to the published version of the manuscript.

Funding

Secretaría de Investigación y Posgrado SIP-20253452-Instituto Politécnico Nacional (IPN), Mexico.

Institutional Review Board Statement

Not applicable.

Informed Consent Statement

Not applicable.

Data Availability Statement

Not applicable.

Acknowledgments

S.-K.K. would like to acknowledge the funding agency of Instituto Politécnico Nacional (IPN) SIP-20253452 and CICATA Altamira, Tamaulipas, Mexico. WA extends gratitude to SECIHTI for the Postdoctoral scholarship provided (Grant number: 878025).

Conflicts of Interest

The authors declare no conflict of interest.

References

1. Yadav, C.S.; Azad, I.; Khan, A.R.; et al. Carbon allotropes: Past to present aspects. In *Biosensors Based on Graphene, Graphene Oxide and Graphynes for Early Detection of Cancer*; CRC Press: Boca Raton, FL, USA, 2025; pp. 1–23.
2. Mauter, M.S.; Elimelech, M. Environmental applications of carbon-based nanomaterials. *Environ. Sci. Technol.* **2008**, *42*, 5843–5859.
3. Sabina-Delgado, A.; Kamaraj, S.K.; Hernández-Montoya, V.; et al. Novel carbon-ceramic composite membranes with high cation exchange properties for use in microbial fuel cell and electricity generation. *Int J Hydrogen Energy* **2023**, *48*, 25512–25526.
4. Kang, J.; Yang, X.; Hu, Q.; et al. Recent progress of amorphous nanomaterials. *Chem. Rev.* **2023**, *123*, 8859–8941.
5. Duan, X.; Tian, W.; Zhang, H.; et al. sp^2/sp^3 framework from diamond nanocrystals: A key bridge of carbonaceous structure to carbocatalysis. *ACS Catal.* **2019**, *9*, 7494–7519.
6. Ike, S.; Vander Wal, R. Effect of carbonization methods on graphitization of soft and hard carbons. *Carbon Trends* **2024**, *16*, 100382. https://doi.org/10.1016/j.cartre.2024.100382.
7. Pozio, A.; Di Carli, M.; Aurora, A.; et al. Hard Carbons for Use as Electrodes in Li-S and Li-ion Batteries. *Nanomaterials* **2022**, *12*, 1349. https://doi.org/10.3390/nano12081349.
8. Ren, X.; Hussain, M.I.; Chang, Y.; et al. State-of-the-Art review on amorphous carbon nanotubes: Synthesis, structure, and application. *Int. J. Mol. Sci.* **2023**, *24*, 17239.
9. Tejasvi, R. Properties of Carbon-Based Nanomaterials and Techniques for Characterization. In *Carbon-Based Nanomaterials for Green Applications*; Wiley: Hoboken, NJ, USA, 2024; pp. 21–55.
10. Ugwumadu, C.; Olson, R. III; Smith, N.L.; et al. Computer simulation of carbonization and graphitization of coal. *Nanotechnology* **2023**, *35*, 095703.
11. Ouzilleau, P.; Gheribi, A.; Chartrand, P. The graphitization temperature threshold analyzed through a second-order structural transformation. *Carbon* **2016**, *109*, 896–908.
12. Goswami, A.D.; Trivedi, D.H.; Jadhav, N.L.; et al. Sustainable and green synthesis of carbon nanomaterials: A review. *J. Environ. Chem. Eng.* **2021**, *9*, 106118.
13. Tu, J.; Wang, X.; Jiang, L.; et al. Efficient graphitization conversion strategies of low-value carbonaceous resources into advanced graphitic carbons. *Chem. Eng. J.* **2025**, *505*, 159472.
14. Aswathappa, S.; Dhas, S.S.; Kumar, R.S. Acoustic shock wave-induced sp^2-to-sp^3-type phase transition-part II: Evidence of the presence of diamond from valance band spectra and electronic diffraction pattern. *Diam. Relat. Mater.* **2024**, *150*, 111680.
15. Chen, C.; Xie, L. Graphene and Graphdiyne. In *Carbon Catalysis*; CRC Press: Boca Raton, FL, USA, 2024; pp. 149–214.
16. Sheka, E.F.; Golubev, Y.A.; Popova, N.A. Amorphous state of sp^2 solid carbon. *Fuller. Nanotub. Carbon Nanostruct.* **2021**, *29*, 107–113.
17. Basit, M.A.; Zafar, R.; Haider, N. Properties of Diamond-like Carbon Coatings. *Appl. Diam.-Like Carbon Coat.* **2025**, *4*, 71–106.
18. Tripathi, N.; Sharma, P.; Pavelyev, V.; et al. A detailed study on carbon nanotubes: Properties, synthesis, and characterization. In *Chemically Modified Carbon Nanotubes for Commercial Applications*; Wiley: Hoboken, NJ, USA, 2023; pp. 1–49.
19. Reyes-Rodríguez, J.L.; Sathish-Kumar, K.; Solorza-Feria, O. Synthesis and functionalization of green carbon as a Pt catalyst support for the oxygen reduction reaction. *Int J Hydrogen Energy* **2015**, *40*, 17253–17263.

20. Diaz, J.; Monteiro, O.R.; Hussain, Z.; Structure of amorphous carbon from near-edge and extended X-ray absorption spectroscopy. *Phys. Rev. B.* **2007**, *76*, 94201. https://doi.org/10.1103/PhysRevB.76.094201.
21. Phua, E.J.; Kai, T.Y.; Woon, L.Y.; et al. Ultra-Thin ta-C Hermetic Seals for Electronics Packaging. In Proceedings of the 2024 IEEE 26th Electronics Packaging Technology Conference (EPTC), Singapore, 3–6 December 2024; pp. 828–835.
22. Shunin, Y.; Bellucci, S.; Gruodis, A.; et al. General Approach to the Description of Fundamental Properties of Disordered Nanosized Media. In *Nonregular Nanosystems: Theory and Applications*; Springer International Publishing: Cham, Switzerland, 2017; pp. 7–31.
23. Odusanya, A.; Rahaman, I.; Sarkar, P.K.; et al. Laser-Assisted Growth of Carbon-Based Materials by Chemical Vapor Deposition. *C* **2022**, *8*, 24.
24. Li, J.; Yin, D.; Qin, Y. Carbon materials: Structures, properties, synthesis and applications. *Manuf. Rev.* **2023**, *10*, 13.
25. Obadero, A.S. Intercalation in Graphite Materials. Ph.D. Thesis, Université Grenoble Alpes, Grenoble, France, 2020.
26. Yang, P.J.; Li, T.H.; Li, H.; et al. Progress in the graphitization and applications of modified resin carbons. *New Carbon Mater.* **2023**, *38*, 96–108.
27. Cao, D.; Wang, L.; Ding, Z.; et al. Characterization of the heterogeneous evolution of the nanostructure of coal-based graphite. *J. Nanosci. Nanotechnol.* **2021**, *21*, 670–681.
28. Hunter, R.D.; Ramírez-Rico, J.; Schnepp, Z. Iron-catalyzed graphitization for the synthesis of nanostructured graphitic carbons. *J. Mater. Chem. A* **2022**, *10*, 4489–4516.
29. Sun, J.; Dang, Y.; Sun, X.; et al. Can carbon be used as an anode for water splitting? *ChemSusChem* **2025**, *18*, e202401340.
30. Ghosh, S.; Zaid, M.; Dutta, J.; et al. Soft carbon in non-aqueous rechargeable batteries: A review of its synthesis, carbonization mechanism, characterization, and multifarious applications. *Energy Adv.* **2024**, *3*, 1167–1195. https://doi.org/10.1039/D4YA00174E.
31. Presser, V.; Heon, M.; Gogotsi, Y. Carbide-derived carbons–from porous networks to nanotubes and graphene. *Adv. Funct. Mater.* **2011**, *21*, 810–833.
32. Bhattacharyya, S. *Carbon Superstructures: From Quantum Transport to Quantum Computation*; CRC Press: Boca Raton, FL, USA, 2024; pp. 1–326.
33. Yuan, G.; Li, B.; Li, X.; et al. Effect of Liquid Crystalline Texture of Mesophase Pitches on the Structure and Property of Large-Diameter Carbon Fibers. *ACS Omega* **2019**, *4*, 1095–1102. https://doi.org/10.1021/acsomega.8b03189.
34. Li, H.; Li, X.; Wei, J.; et al. Crystalline transformation from ta-C to graphene induced by a catalytic Ni layer during annealing. *Diam. Relat. Mater.* **2020**, *101*, 107556.
35. Loh, G.C.; Baillargeat, D. Graphitization of amorphous carbon and its transformation pathways. *J. Appl. Phys.* **2013**, *114*, 033534.
36. Zhao, Y.; Zhao, C.; Wang, X.; et al. Stability of sp Hybridized Amorphous Carbon and its Transformation to Nanodiamond. *Small Methods* **2025**, *9*, 2500294.
37. Konicek, A.R.; Grierson, D.S.; Gilbert, P.U.P.A.; et al. Origin of Ultralow Friction and Wear in Ultrananocrystalline Diamond. *Phys. Rev. Lett.* **2008**, *100*, 235502.
38. Thapa, R.; Ugwumadu, C.; Nepal, K.; et al. Ab Initio Simulation of Amorphous Graphite. *Phys. Rev. Lett.* **2022**, *128*, 236402.
39. Gomez-Martin, A.; Schnepp, Z.; Ramirez-Rico, J. Structural Evolution in Iron-Catalyzed Graphitization of Hard Carbons. *Chem. Mater.* **2021**, *33*, 3087–3097.
40. Kupka, K.; Leino, A.; Ren, W.; et al. Graphitization of Amorphous Carbon by Swift Heavy Ion Impacts: Molecular Dynamics Simulation. *Diam. Relat. Mater.* **2018**, *83*, 134–140.
41. Li, K.; Zhang, H.; Li, G.; et al. ReaxFF Molecular Dynamics Simulation for the Graphitization of Amorphous Carbon: A Parametric Study. *J. Chem. Theory Comput.* **2018**, *14*, 2322–2331.
42. Liu, Y.; Gao, T.; Xiao, Q.; et al. Generalized modeling of carbon film deposition growth via hybrid MD/MC simulations with machine-learning potentials. *NPJ Comput. Mater.* **2025**, *11*, 285.
43. Amini, S.; Abbaschian, R. Nucleation and growth kinetics of graphene layers from a molten phase. *Carbon* **2013**, *51*, 110–123. https://doi.org/10.1016/j.carbon.2012.08.019.
44. Boubiche, N.; El Hamouchi, J.; Hulik, J.; et al. Kinetics of Graphitization of thin diamond-like carbon (DLC) films catalyzed by transition metal. *Diam. Relat. Mater.* **2019**, *91*, 190–198.
45. Rigollet, S.; Weiss-Hortala, E.; Flamant, G.; et al. Biocarbon graphenization processes and energy assessment. *A Rev. Chem. Eng. J.* **2024**, *496*, 153795. https://doi.org/10.1016/j.cej.2024.153795.
46. Thambiliyagodage, C.J.; Ulrich, S.; Araujo, P.T.; et al. Catalytic graphitization in nanocast carbon monoliths by iron, cobalt and nickel nanoparticles. *Carbon* **2018**, *134*, 452–463.
47. Abdullah, N.R.; Rashid, H.O.; Tang, C.S.; et al. Controlling physical properties of bilayer graphene by stacking orientation caused by interaction between B and N dopant atoms. *Mater. Sci. Eng. B* **2022**, *276*, 115554.
48. Liu, C.; Fang, W.; Cheng, Q.; et al. Revolutionizing elastomer technology: Advances in reversible crosslinking, reprocessing, and self-healing applications. *Polym. Rev.* **2025**, *65*, 483–526.

49. Wang, M.X. Nitrogen and oxygen bridged calixaromatics: Synthesis, structure, functionalization, and molecular recognition. *Acc. Chem. Res.* **2012**, *45*, 182–195.
50. McLean, B.; Webber, G.; Page, A. Boron Nitride Nucleation Mechanism during Chemical Vapor Deposition. *J. Phys. Chem. C* **2018**, *122*, 24341–24349. https://doi.org/10.1021/acs.jpcc.8b05785.
51. Fan, X.; Dong, X.; Wei, W.H.; et al. Monitoring single-heteroatom loss during deoxygenation and denitrogenation of soluble organic matter in coal using mass spectrometric methods. *Fuel* **2021**, *292*, 120294.
52. Gür, T.M. Review of electrical energy storage technologies, materials and systems: Challenges and prospects for large-scale grid storage. *Energy Environ. Sci.* **2018**, *11*, 2696–2767.
53. McKee, D.W. Oxidation protection of carbon materials. In *Chemistry & Physics of Carbon*; Boca Raton, FL, USA, 2021; pp. 173–232.
54. Li, S.; Liu, J.; Chen, Y.; et al. Graphitization Induction Effect of Hard Carbon for Sodium-Ion Storage. *Adv. Funct. Mater.* **2025**, *35*, 2424629.
55. Devi, M.; Wang, H.; Moon, S.; et al. Laser-Carbonization–A powerful tool for micro-fabrication of patterned electronic carbons. *Adv. Mater.* **2023**, *35*, 2211054.
56. Inagaki, M.; Kaburagi, Y.; Hishiyama, Y. Thermal management material: Graphite. *Adv. Eng. Mater.* **2014**, *16*, 494–506.
57. Ren, K.; Liu, Z.; Wei, T.; et al. Recent developments of transition metal compounds-carbon hybrid electrodes for high energy/power supercapacitors. *Nano-Micro Lett.* **2021**, *13*, 129.
58. Goronzy, D.P.; Ebrahimi, M.; Rosei, F.; et al. Supramolecular assemblies on surfaces: Nanopatterning, functionality, and reactivity. *ACS Nano* **2018**, *12*, 7445–7481.
59. Izatt, R.M.; Izatt, S.R.; Izatt, N.E.; et al. Industrial applications of molecular recognition technology to separations of platinum group metals and selective removal of metal impurities from process streams. *Green Chem.* **2015**, *17*, 2236–2245.
60. Xu, R.; Du, L.; Adekoya, D.; et al. Well-defined nanostructures for electrochemical energy conversion and storage. *Adv. Energy Mater.* **2021**, *11*, 2001537.
61. Li, X.Y.; Zhang, Z.H.; Cheng, X.W.; et al. The development and application of spark plasma sintering technique in advanced metal structure materials: A review. *Powder Metall. Met. Ceram.* **2021**, *60*, 410–438.
62. Zhu, W.; Zhu, L. Argon-assisted electrical explosion of graphite powder in a constraint tube: Experimental and MD insights into the exfoliation mechanism. *Ceram. Int.* **2025**, *51*, 21689–21701.
63. Taqy, S.; Haque, A. Radiation-induced synthesis of carbon nanostructures. In *Handbook of Functionalized Carbon Nanostructures: From Synthesis Methods to Applications*; Springer International Publishing: Cham, Switzerland, 2024; pp. 729–788.
64. Sathish-Kumar, K.; Vázquez-Huerta, G.; Rodríguez-Castellanos, A.; et al. Microwave Assisted Synthesis and Characterizations of Decorated Activated Carbon. *Int. J. Electrochem. Sci.* **2012**, *7*, 5484–5494.
65. Krasheninnikov, A.V.; Banhart, F.J. Engineering of nanostructured carbon materials with electron or ion beams. *Nat. Mater.* **2007**, *6*, 723–733.
66. Schwenke, A.M.; Hoeppener, S.; Schubert, U.S. Synthesis and modification of carbon nanomaterials utilizing microwave heating. *Adv. Mater.* **2015**, *27*, 4113–4141.
67. Ramasundaram, S.; Jeevanandham, S.; Vijay, N.; et al. Unraveling the Dynamic Properties of New-Age Energy Materials Chemistry Using Advanced In Situ Transmission Electron Microscopy. *Molecules* **2024**, *29*, 4411.
68. Nakamura, Y.; Yoshino, T.; Satish-Kumar, M. Pressure dependence of graphitization: Implications for rapid recrystallization of carbonaceous material in a subduction zone. *Contrib. Mineral. Petrol.* **2020**, *175*, 32.
69. Mishra, S.; Datta, R. Embrittlement of Steel. In *Encyclopedia of Materials: Science and Technology*; Buschow, K.H.J., Cahn, R.W., Flemings, M.C., et al., Eds.; Elsevier: Amsterdam, The Netherlands, 2001; pp. 2761–2768.
70. Mostafavi, E.; Iravani, S.; Varma, R.S.; et al. Eco-friendly synthesis of carbon nanotubes and their cancer theranostic applications. *Mater. Adv.* **2022**, *3*, 4765–4782.
71. Choi, G.B.; Ahn, J.-R.; Kim, J.; et al. Unraveling the Catalytic Graphitization Mechanism of Ni–P Electroless Plated Cokes via In Situ Analytical Approaches. *ACS Omega* **2024**, *9*, 6741–6748.
72. Kuzovkov, V.; Kotomin, E.; Vila, R. Theoretical analysis of thermal annealing kinetics of radiation defects in silica. *J. Nucl. Mater.* **2023**, *579*, 154381. https://doi.org/10.1016/j.jnucmat.2023.154381.
73. Xu, X.; Cao, D.; Wei, Y.; et al. Impact of Graphitization Degree on the Electrochemical and Thermal Properties of Coal. *ACS Omega* **2024**, *9*, 2443–2456. https://doi.org/10.1021/acsomega.3c06871.
74. Yan, Q.; Xin, Y.; Zhang, X.; et al. Effect of graphitization temperature on microstructure, mechanical and ablative properties of C/C composites with pitch and pyrocarbon dual-matrix. *Ceram. Int.* **2022**, *49*, 2860–2870. https://doi.org/10.1016/j.ceramint.2022.09.269.
75. Chen, C.; Sun, K.; Wang, A.; et al. Catalytic graphitization of cellulose using nickel as catalyst. *BioResources* **2018**, *13*, 3165–3176.

76. Jeon, C.; Hwang, S.; Han, M.; et al. Unveiling the graphitization behaviors of highly stiff and thermally conductive graphitic carbon fibers. *Carbon* **2025**, *245*, 120791.
77. Shokrani Havigh, R.; Mahmoudi Chenari, H. A comprehensive study on the effect of carbonization temperature on the physical and chemical properties of carbon fibers. *Sci. Rep.* **2022**, *12*, 10704. https://doi.org/10.1038/s41598-022-15085-x.
78. Clarke, A.P. Catalytic Methane Chemistry in High-Temperature Molten Environments. Ph.D. Thesis, University of California, Berkeley, CA, USA, 2021.
79. Pusarapu, V.; Narayana Sarma, R.; Ochonma, P.; et al. Sustainable co-production of porous graphitic carbon and synthesis gas from biomass resources. *NPJ Mater. Sustain.* **2024**, *2*, 16. https://doi.org/10.1038/s44296-024-00020-0.
80. Lower, L.; Dey, S.; Vook, T.; et al. Catalytic Graphitization of Biocarbon for Lithium-Ion Anodes: A Minireview. *ChemSusChem* **2023**, *16*, e202300729.
81. Liu, P.; Du, W.; Liu, X.; et al. Sustainable catalytic graphitization of biomass to graphitic porous carbon by constructing permeation network with organic ligands. *Chin. J. Chem. Eng.* **2023**, *64*, 259–270. https://doi.org/10.1016/j.cjche.2023.06.025.
82. Shi, M.; Song, C.; Tai, Z.; et al. Coal-derived synthetic graphite with high specific capacity and excellent cyclic stability as anode material for lithium-ion batteries. *Fuel* **2021**, *292*, 120250. https://doi.org/10.1016/j.fuel.2021.120250.
83. Tung, T.T.; Pereira, A.L.C.; Poloni, E.; et al. Irradiation methods for engineering of graphene related two-dimensional materials. *Appl. Phys. Rev.* **2023**, *10*, 031309. https://doi.org/10.1063/5.0148376.
84. Frankenstein, L.; Glomb, P.; Ramirez-Rico, J.; et al. Revealing the Impact of Different Iron-Based Precursors on the 'Catalytic' Graphitization for Synthesis of Anode Materials for Lithium Ion Batteries. *ChemElectroChem* **2023**, *10*, e202201073.
85. Shang, T.; Zhan, H.; Gong, Q.; et al. Insights into the thermal and electric field distribution and the structural optimization in the graphitization furnace. *Energy* **2024**, *297*, 131269.
86. Acedera, R. How Does Graphitization Affect the Structure and Properties of Carbon Fiber Papers? 2023. Available online: https://blog.caplinq.com/how-does-graphitization-affect-the-structure-and-properties-of-carbon-fiber-papers_4869/ (accessed on 14 September 2025).
87. Yoshihiro, N.; Takashi, Y.; Sathish, M. An experimental kinetic study on the structural evolution of natural carbonaceous material to graphite. *Am. Mineral.* **2017**, *102*, 135–148
88. Zhang, G.; Wen, M.; Wang, S.; et al. Insights into thermal reduction of the oxidized graphite from the electro-oxidation processing of nuclear graphite matrix. *RSC Adv.* **2018**, *8*, 567–579. https://doi.org/10.1039/C7RA11578D.
89. Marin, D.; Marchesan, S. Carbon Graphitization: Towards Greener Alternatives to Develop Nanomaterials for Targeted Drug Delivery. *Biomedicines* **2022**, *10*, 1320. https://doi.org/10.3390/biomedicines10061320.
90. Li, J.; Cheng, T.; Wu, H.; et al. CO_2-assisted synthesis of graphitic resin-based activated carbon for ultrahigh selective adsorption of VOCs under humid conditions. *Fuel* **2023**, *353*, 129157. https://doi.org/10.1016/j.fuel.2023.129157.
91. Islam, F.; Tahmasebi, A.; Wang, R.; et al. Structure of Coal-Derived Metal-Supported Few-Layer Graphene Composite Materials Synthesized Using a Microwave-Assisted Catalytic Graphitization Process. *Nanomaterials* **2021**, *11*, 1672. https://doi.org/10.3390/nano11071672.
92. Shi, Z.; Wang, Y.; Lu, M.; et al. Catalytic graphitization of engineered pyrolysis bio-oil for sustainable graphite and hydrogen Co-production. *Renew. Energy* **2026**, *256*, 124149. https://doi.org/10.1016/j.renene.2025.124149.
93. Chen, X.; Deng, X.; Kim, N.Y.; et al. Graphitization of graphene oxide films under pressure. *Carbon* **2018**, *132*, 294–303.
94. Gentile, M.; Bellani, S.; Zappia, M.I.; et al. Hydrogen-Assisted Thermal Treatment of Electrode Materials for Electrochemical Double-Layer Capacitors. *ACS Appl. Mater. Interfaces* **2024**, *16*, 13706–13718. https://doi.org/10.1021/acsami.3c18629.
95. Zhao, J.G.; Li, F.Y.; Jin, C.Q. Graphitization of activated carbon under high pressures and high temperatures. *Solid State Commun.* **2009**, *149*, 818–821. https://doi.org/10.1016/j.ssc.2008.12.027.
96. Oluwole, O.S.; Jovanović; P; Mohonta, S.C.; et al. Low-temperature graphitization by amine-assisted combustion of graphite oxide. *NPJ 2d Mater. Appl.* **2025**, *9*, 52. https://doi.org/10.1038/s41699-025-00572-2.
97. Padwal, C.; Wang, X.; Pham, H.D.; et al. Efficient and swift heating technique for crafting highly graphitized carbon and crystalline silicon (Si@GC) composite anodes for lithium-ion batteries. *Battery Energy* **2024**, *3*, 20240025. https://doi.org/10.1002/bte2.20240025.
98. Lazareva, I.; Koval, Y.; Alam, M.; et al. Graphitization of polymer surfaces by low-energy ion irradiation. *Appl. Phys. Lett.* **2007**, *90*, 262108. https://doi.org/10.1063/1.2752738.
99. Antonelou, A.; Sygellou, L.; Vrettos, K.; et al. Efficient defect healing and ultralow sheet resistance of laser-assisted reduced graphene oxide at ambient conditions. *Carbon* **2018**, *139*, 492–499. https://doi.org/10.1016/j.carbon.2018.07.012.
100. Claro, P.I.C.; Pinheiro, T.; Silvestre, S.L.; et al. Sustainable carbon sources for green laser-induced graphene: A perspective on fundamental principles, applications, and challenges. *Appl. Phys. Rev.* **2022**, *9*, 041305. https://doi.org/10.1063/5.0100785.
101. Baghel, P.; Sakhiya, A.K.; Kaushal, P. Ultrafast growth of carbon nanotubes using microwave irradiation: Characterization and its potential applications. *Heliyon* **2022**, *8*, e10943. https://doi.org/10.1016/j.heliyon.2022.e10943.
102. Jones, L.; Goffin, N.; Ouyang, J.; et al. Laser specific energy consumption: How do laser systems compare to other manufacturing processes? *J. Laser Appl.* **2022**, *34*, 42029. https://doi.org/10.2351/7.0000790.

103. Olejnik, A.; Polaczek, K.; Szkodo, M.; et al. Laser-Induced Graphitization of Polydopamine on Titania Nanotubes. *ACS Appl. Mater. Interfaces* **2023**, *15*, 52921–52938. https://doi.org/10.1021/acsami.3c11580.
104. Kim, J.; Son, S.; Choe, M.; et al. In situ TEM investigation of nickel catalytic graphitization. *Mater. Today Adv.* **2024**, *22*, 100494. https://doi.org/10.1016/j.mtadv.2024.100494.
105. Shyam Kumar, C.N.; Chakravadhanula, V.S.K.; Riaz, A.; et al. Understanding Graphitization and Growth of free-standing Nanocrystalline Graphene using In Situ Transmission Electron Microscopy. *Nanoscale* **2017**, *9*, 12835–12842. https://doi.org/10.1039/C7NR03276E.
106. Zhang, F.; Liu, W. Recent progress of operando transmission electron microscopy in heterogeneous catalysis. *Microstructures* **2024**, *4*, 202404. https://doi.org/10.20517/microstructures.2024.03.
107. Schito, A.; Muirhead, D.K.; Parnell, J. Towards a kerogen-to-graphite kinetic model by means of Raman spectroscopy. *Earth-Sci. Rev.* **2023**, *237*, 104292. https://doi.org/10.1016/j.earscirev.2022.104292.
108. Gao, Y.; Zou, C.; She, Y.; et al. Analysis of Structural Heterogeneity in Low-Rank Coal and Its Pyrolyzed Char Using Multi-Point Scanning Micro-Raman Spectroscopy. *Molecules* **2024**, *29*, 2361. https://doi.org/10.3390/molecules29102361.
109. Zerda, T.; Gruber, T. Raman Study of Kinetics of Graphitization of Carbon Blacks. *Rubber Chem. Technol.* **2000**, *73*, 284–292. https://doi.org/10.5254/1.3547591.
110. Huali, W.; Ruchi, G.; Allen, C.; et al. Comparative Analysis of Microstructure and Reactive Sites for Nuclear Graphite IG-110 and Graphite Matrix A3. *J. Nucl. Mater.* **2020**, *528*, 151802.
111. Jaiswal, K.K.; Chowdhury, C.R.; Yadav, D.; et al. Renewable and sustainable clean energy development and impact on social, economic, and environmental health. *Energy Nexus* **2022**, *7*, 100118. https://doi.org/10.1016/j.nexus.2022.100118.
112. Kim, T.; Lee, J.; Lee, K.-H. Full graphitization of amorphous carbon by microwave heating. *RSC Adv.* **2016**, *6*, 24667–24674. https://doi.org/10.1039/C6RA01989G.
113. Islam, F.; Wang, J.; Tahmasebi, A.; et al. Microwave-Assisted Coal-Derived Few-Layer Graphene as an Anode Material for Lithium-Ion Batteries. *Materials* **2021**, *14*, 6468. https://doi.org/10.3390/ma14216468.
114. Liang, C.; Chen, Y.; Wu, M.; et al. Green synthesis of graphite from CO_2 without graphitization process of amorphous carbon. *Nat. Commun.* **2021**, *12*, 119. https://doi.org/10.1038/s41467-020-20380-0.
115. Shi, Z.; Wang, S.; Jin, Y.; et al. Establishment of green graphite industry: Graphite from biomass and its various applications. *SusMat* **2023**, *3*, 402–415. https://doi.org/10.1002/sus2.139.
116. Sruthy, S.; Grimm, A.; Paul, M.; et al. Low-temperature Highly Graphitized Porous Biomass-based Carbon as an Efficient and Stable Electrode for Lithium-ion Batteries and Supercapacitors. *Chem. Eng. J. Adv.* **2025**, *22*, 100762. https://doi.org/10.1016/j.ceja.2025.100762.
117. Zhao, H.; Wu, H.; Rong, T.; et al. Green and efficient graphitization of biomass waste empowered by molten salt electrolysis: Mechanistic exploration and energy storage applications dual-driven by experiments and simulations. *J. Mater. Chem. A* **2025**, *13*, 3777–3790. https://doi.org/10.1039/D4TA07890J.
118. Li, K.; Liu, Q.; Cheng, H.; et al. Classification and carbon structural transformation from anthracite to natural coaly graphite by XRD, Raman spectroscopy, and HRTEM. *Spectrochim. Acta Part A Mol. Biomol. Spectrosc.* **2021**, *249*, 119286.
119. Pardanaud, C.; Cartry, G.; Lajaunie, L.; et al. Investigating the possible origin of Raman bands in defective sp^2/sp^3 carbons below 900 cm^{-1}: Phonon density of states or double resonance mechanism at play? *C* **2019**, *5*, 79.
120. Li, G.; Zhang, H.; Han, Y. Applications of transmission electron microscopy in phase engineering of nanomaterials. *Chem. Rev.* **2023**, *123*, 10728–10749.
121. Su, Y.F.; Park, J.G.; Koo, A.; et al. Characterization at atomic resolution of carbon nanotube/resin interface in nanocomposites by mapping sp^2-bonding states using electron energy-loss spectroscopy. *Microsc. Microanal.* **2016**, *22*, 666–672.
122. Vander Wal, R.L.; Bryg, V.M.; Hays, M.D. XPS analysis of combustion aerosols for chemical composition, surface chemistry, and carbon chemical state. *Anal. Chem.* **2011**, *83*, 1924–1930.
123. Seki, S.; Paitandi, R.P.; Choi, W.; et al. Electron transport over 2D molecular materials and assemblies. *Acc. Chem. Res.* **2024**, *57*, 2665–2677.
124. Munir, K.S.; Wen, C. Deterioration of the strong sp^2 carbon network in carbon nanotubes during the mechanical dispersion processing—A review. *Crit. Rev. Solid State Mater. Sci.* **2016**, *41*, 347–366.
125. Mennani, M.; Ait Benhamou, A.; Mekkaoui, A.A.; et al. Probing the evolution in catalytic graphitization of biomass-based materials for enduring energetic applications. *J. Mater. Chem. A* **2024**, *12*, 6797–6825.
126. Li, N.; Li, X.; Wang, T.; et al. In situ transmission electron microscopy characterization and manipulation of the morphology, composition and phase evolution of nanomaterials under microenvironmental conditions. *Chem. Sci.* **2025**, *16*, 9604–9637.
127. Li, J.; Qin, Y.; Chen, Y.; et al. Structural characteristics and evolution of meta-anthracite to coaly graphite: A quantitative investigation using X-ray diffraction, Raman spectroscopy, and high-resolution transmission electron microscopy. *Fuel* **2023**, *333*, 126334.

128. Xue, B.; Ye, J.; Zhang, J. Highly conductive Poly (L-lactic acid) composites obtained via in situ expansion of graphite. *J. Polym. Res.* **2015**, *22*, 112.
129. Shi, Z.; Jin, Y.; Han, T.; et al. Bio-based anode material production for lithium–ion batteries through catalytic graphitization of biochar: The deployment of hybrid catalysts. *Sci. Rep.* **2024**, *14*, 3966. https://doi.org/10.1038/s41598-024-54509-8.
130. Guan, L.; Li, D.; Ji, S.; et al. Structural Regulation and Performance Enhancement of Carbon-Based Supercapacitors: Insights into Electrode Material Engineering. *Materials* **2025**, *18*, 456. https://doi.org/10.3390/ma18020456.
131. Hao, J.; Li, J.; Shi, X.; et al. Changes in microstructure and mechanical properties of the carbon fiber and their effects on C/SiC composites. *Mater. Charact.* **2022**, *193*, 112334. https://doi.org/10.1016/j.matchar.2022.112334.
132. Gao, Z.; Zhu, J.; Rajabpour, S.; et al. Graphene reinforced carbon fibers. *Sci. Adv.* **2025**, *6*, eaaz4191. https://doi.org/10.1126/sciadv.aaz4191.
133. Li, R.; Hu, J.; Li, Y.; et al. Graphene-Based, Flexible, Wearable Piezoresistive Sensors with High Sensitivity for Tiny Pressure Detection. *Sensors* **2025**, *25*, 423. https://doi.org/10.3390/s25020423.
134. Rzeźniczak, P.; Skrzetuska, E.; Venkataraman, M.; et al. Influence of the Ozonation Process on Expanded Graphite for Textile Gas Sensors. *Sensors* **2025**, *25*, 5328. https://doi.org/10.3390/s25175328.
135. Roselin, L.S.; Juang, R.S.; Hsieh, C.T.; et al. Recent advances and perspectives of carbon-based nanostructures as anode materials for Li-ion batteries. *Materials* **2019**, *12*, 1229.
136. Ávila Vázquez, V.; Enciso Hernández, E.A.; Kamaraj, S.K.; et al. Use of activated carbon and camphor carbon as cathode and clay cup as proton exchange membrane in a microbial fuel cell for the bioenergy production from crude glycerol biodegradation. *J. Environ. Sci. Health Part A* **2022**, *57*, 947–957.
137. Wang, G.; Yu, M.; Feng, X. Carbon materials for ion-intercalation involved rechargeable battery technologies. *Chem. Soc. Rev.* **2021**, *50*, 2388–2443.
138. He, J.; Zhang, D.; Wang, Y.; et al. Biomass-derived porous carbons with tailored graphitization degree and pore size distribution for supercapacitors with ultra-high rate capability. *Appl. Surf. Sci.* **2020**, *515*, 146020.
139. Xia, Y.; Yang, Z.; Zhu, Y. Porous carbon-based materials for hydrogen storage: Advancement and challenges. *J. Mater. Chem. A* **2013**, *1*, 9365–9381.
140. Liu, J.; Huang, L.; Wang, H.; et al. The origin, characterization, and precise design and regulation of diverse hard carbon structures for targeted applications in lithium-/sodium-/potassium-ion batteries. *Electrochem. Energy Rev.* **2024**, *7*, 34.
141. Shao, Y.; Hourdin, L.; Sanchez, J.-Y.; et al. Fluorinated materials in electrochemical storage and conversion devices: assessment of advantages and disadvantages. *C. R. Chimie* **2025**, 28, 523–541.
142. Hecht, D.S.; Hu, L.; Irvin, G. Emerging transparent electrodes based on thin films of carbon nanotubes, graphene, and metallic nanostructures. *Adv. Mater.* **2011**, *23*, 1482–1513.
143. Xu, J.; Wang, Y.; Hu, S. Nanocomposites of graphene and graphene oxides: Synthesis, molecular functionalization and application in electrochemical sensors and biosensors: A review. *Microchim. Acta* **2017**, *184*, 1–44.
144. Raagulan, K.; Kim, B.M.; Chai, K.Y. Recent advancement of electromagnetic interference (EMI) shielding of two dimensional (2D) MXene and graphene aerogel composites. *Nanomaterials* **2020**, *10*, 702.
145. Fredj, Z.; Sawan, M. Advanced Nanomaterials-Based Electrochemical Biosensors for Catecholamines Detection: Challenges and Trends. *Biosensors* **2023**, *13*, 211.
146. Ma, Z.; Wang, W.; Xiong, Y.; et al. Carbon Micro/Nano Machining toward Miniaturized Device: Structural Engineering, Large-Scale Fabrication, and Performance Optimization. *Small* **2024**, *21*, 2400179.
147. Sayam, A.; Rahman, A.M.; Rahman, M.S.; et al. A review on carbon fiber-reinforced hierarchical composites: Mechanical performance, manufacturing process, structural applications and allied challenges. *Carbon Lett.* **2022**, *32*, 1173–1205.
148. Ouyang, J.H.; Li, Y.F.; Zhang, Y.Z.; et al. High-temperature solid lubricants and self-lubricating composites: A critical review. *Lubricants* **2022**, *10*, 177.
149. Hassan, S.; Nadeem, A.Y.; Qaiser, H.; et al. A review of carbon-based materials and their coating techniques for biomedical implants applications. *Carbon Lett.* **2023**, *33*, 1171–1188.
150. Liu, Y.; Yang, J.; Wang, M.; et al. Recent developments in interface engineering strategies for stabilizing sodium metal anodes. *Cell Rep. Phys. Sci.* **2024**, *5*.
151. Zhou, X.; Qiao, J.; Yang, L.; et al. A review of graphene-based nanostructural materials for both catalyst supports and metal-free catalysts in PEM fuel cell oxygen reduction reactions. *Adv. Energy Mater.* **2014**, *4*, 1301523.
152. Gopinath, K.P.; Vo, D.V.; Gnana Prakash, D.; et al. Environmental applications of carbon-based materials: A review. *Environ. Chem. Lett.* **2021**, *19*, 557–582.
153. Li, P.; Galek, P.; Grothe, J.; et al. Carbon-based iontronics–current state and future perspectives. *Chem. Sci.* **2025**, *16*, 7130–7154.
154. Alfieri, A.; Anantharaman, S.B.; Zhang, H.; et al. Nanomaterials for quantum information science and engineering. *Adv. Mater.* **2023**, *35*, 2109621.

155. Speranza, G. The role of functionalization in the applications of carbon materials: An overview. *C* **2019**, *5*, 84.
156. Sharma, S.; Basu, S.; Shetti, N.P.; et al. Versatile graphitized carbon nanofibers in energy applications. *ACS Sustain. Chem. Eng.* **2022**, *10*, 1334–1360.
157. Sikder, S.; Toha, M.; Rahman, M.M. Environmental Sustainability and Future Challenges of Waste-Derived Carbon Nanomaterials. In *Waste Derived Carbon Nanomaterials*; American Chemical Society: Washington, DC, USA, 2025; Volume 1, pp. 309–330.
158. Zhou, T.; Wu, X.; Liu, S.; et al. Biomass-derived catalytically active carbon materials for the air electrode of Zn-air batteries. *ChemSusChem* **2024**, *17*, e202301779.
159. Osman, A.I.; Nasr, M.; Mohamed, A.R.; et al. Life cycle assessment of hydrogen production, storage, and utilization toward sustainability. *Wiley Interdiscip. Rev. Energy Environ.* **2024**, *13*, e526.
160. Majumder, A.; Ray, B.C. Energy Efficiency and Sustainability. In *Sinter Plants: Evolution, Challenges, and Future Perspectives*; Springer Nature: Singapore, 2025; pp. 135–169